Available online at www.sciencedirect.com
SCIENCE DIRECT
Journal of Computational Physics 216 (2006) 547–572
JOURNAL OF COMPUTATIONAL PHYSICS
www.elsevier.com/locate/jcp

Integral and integrable algorithms for a nonlinear shallow-water wave equation

Roberto Camassa, Jingfang Huang, Long Lee *

Department of Mathematics, University of North Carolina at Chapel Hill, Philips Hall cb 3250, Chapel Hill, NC 27599, United States

Received 12 May 2005; received in revised form 18 December 2005; accepted 20 December 2005
Available online 8 February 2006

Abstract

An asymptotic higher-order model of wave dynamics in shallow water is examined in a combined analytical and numerical study, with the aim of establishing robust and efficient numerical solution methods. Based on the Hamiltonian structure of the nonlinear equation, an algorithm corresponding to a completely integrable particle lattice is implemented first. Each "particle" in the particle method travels along a characteristic curve. The resulting system of nonlinear ordinary differential equations can have solutions that blow-up in finite time. We isolate the conditions for global existence and prove l_1-norm convergence of the method in the limit of zero spatial step size and infinite particles. The numerical results show that this method captures the essence of the solution without using an overly large number of particles. A fast summation algorithm is introduced to evaluate the integrals of the particle method so that the computational cost is reduced from $O(N^2)$ to $O(N)$, where N is the number of particles. The method possesses some analogies with point vortex methods for 2D Euler equations. In particular, near singular solutions exist and singularities are prevented from occurring in finite time by mechanisms akin to those in the evolution of vortex patches. The second method is based on integro-differential formulations of the equation. Two different algorithms are proposed, based on different ways of extracting the time derivative of the dependent variable by an appropriately defined inverse operator. The integro-differential formulations reduce the order of spatial derivatives, thereby relaxing the stability constraint and allowing large time steps in an explicit numerical scheme. In addition to the Cauchy problem on the infinite line, we include results on the study of the nonlinear equation posed in the quarter (space-time) plane. We discuss the minimum number of boundary conditions required for solution uniqueness and illustrate this with numerical examples.

1. Introduction

The nonlinear partial differential equation (PDE) of evolution

$$u_t + 2\kappa u_x - u_{xxt} + 3uu_x = 2u_x u_{xx} + uu_{xxx} \tag{1.1}$$

results from an asymptotic expansion of the Euler equations governing the motion of an inviscid fluid whose free surface can exhibit gravity driven wave motion [7]. The small parameters used to carry out the expansion

* Corresponding author. Tel.: +1 919 843 2218; fax: +1 919 962 9345.
E-mail address: longlee@email.unc.edu (L. Lee).

0021-9991/$ - see front matter © 2006 Elsevier Inc. All rights reserved.
doi:10.1016/j.jcp.2005.12.013

are the aspect ratio, whereby the depth of the fluid is assumed to be much smaller than the typical wavelength of the motion, and the amplitude ratio, or ratio between a typical amplitude of wave motion and the average depth of the fluid. Thus, the equation is a member of the class of weakly nonlinear (due to the smallness assumption on the amplitude parameter) and weakly dispersive (due to the long wave assumption parameter) models for water wave propagation. However, at variance with its celebrated close relatives in this class, such as the Korteweg–de Vries (KdV) and Benjamin–Bona–Mahony (BBM) equations, these small parameters are assumed to be linked only by a relative ordering, rather than a power law relation. This allows to retain terms on the right hand side that would be of higher order with respect to both the KdV and BBM expansions, and, in principle, consider dynamical regimes in which nonlinearity is somewhat dominant with respect to wave dispersion.

The choice of the dimensional form (1.1) is dictated by its relative simplicity. In fact, the equation written in this way refers to a frame of reference moving at uniform speed, which allows to eliminate extra terms arising from the derivation of the equation in the lab frame of reference (where the fluid can be considered at rest at some boundary). Thus, in the form presented here the dependent variable u refers to the horizontal fluid velocity along the x-direction as measured at time t by an observer moving at speed κ. This speed is related to the critical shallow-water wave speed $\sqrt{gh_0}$, where g is the gravity acceleration and h_0 is the undisturbed water depth.

The physical foundations of Eq. (1.1) are accompanied by some peculiar mathematical features. These have received some attention in the recent literature, and no attempt will be made here to provide a detailed reference list. Suffices to say that, like the KdV model, the equation possesses the remarkable property of complete integrability, as evidenced by its Lax-pair representation. Moreover, this property is complemented by the existence of a class of weak solutions that can serve as a natural projection of the general solution of (1.1) to an approximating (but still completely integrable) finite dimensional dynamical system [7,4]. This system of ordinary differential equations (ODEs) can be viewed as describing particle interacting through a long range potential (here position and momentum dependent), which expresses the fact that such particles are advected by the velocity u of the shallow-water wave equation (1.1). The velocity is in turn determined by the particle positions and momenta.

A curious property of Eq. (1.1) is that it can be written in a form reminiscent of the Euler equations governing the dynamics of an incompressible fluid [14] (cf. Eq. (6.7) in Section 6.1). The particle system for Eq. (1.1) can then be interpreted as a (much simpler) counterpart of the various point vortex formulations for Euler equations. Of course, this "point vortex" system resulting from Eq. (1.1) has the added bonus of inheriting the complete integrability of the continuum equation, so that in principle a closed form expression for the solution is available. However, the practical usage of this expression is unclear as the number of particles grows. It is then natural to attempt to use the particle system as the starting point for a numerical method to solve Eq. (1.1) [4].

The present work focuses on developing and analyzing such a numerical scheme. To test this method and provide simultaneous benchmarking, we also introduce more general PDE-like numerical methods, while still taking advantage of the structure of the equation, which relies on the nonlocal operator $(1-\partial_x^2)^{-1}$ for its formulation. Our emphasis is on simplicity and efficiency, rather than high-order accuracy, though some higher accuracy can be achieved with a modicum of extra effort.

We develop the particle method first. Specifically, in Section 2 we review the integrable formulation for the shallow-water wave equation (1.1) and show how the particle method arises from this formulation in a straightforward manner. We then establish the properties of the method from the viewpoint of ODEs in a series of propositions, and, in particular, show that for a relatively wide class of initial data there are no particle collisions in finite times. We then go on to prove convergence of the particle method in Section 4. Next, Section 5 improves the particle algorithm by implementing a fast summation to reduce the computational cost from $O(N^2)$ to $O(N)$, where N is the number of particles. Sections 5.1 and 5.2 present a few tests of the particle method. The tests for the case $\kappa = 0$ show evidence of instability, which turns out to be related to clustering of particles, in theory forbidden for finite times but in practice occurring due to the exponentially fast decay of inter-particle distance. A simple redistribution algorithm to prevent instabilities of this kind is then introduced in Section 5.3. The analogy with Euler equations mentioned above is carried further in Section 5.5, where we show that the emergence, under certain conditions, of peaked solutions of Eq. (1.1) from smooth initial data can be viewed as a cartoon of the near-singular behavior in the evolution of vortex patches [8,2,25].

In Section 6 we introduce integral formulations and discuss their numerical implementations. Using appropriately defined integral operators, the nonlinear equation (1.1) gives rise to two equivalent integro-differential

equations. An immediate advantage of such integral forms is the reduced order of spatial derivatives. This relaxes the stability constraint and thus allows the use of larger time steps in an explicit marching scheme. Also, using local correction ideas similar to [28], we present a higher order numerical quadrature for the integral. Compared with the particle method where $2N$ variables (N each, respectively, for positions and momenta) are updated at each time step, the integral formulations use only N unknowns (given N grid points). However, the particle method is naturally adaptive, and numerical results for the case of emerging sharply peaked waves ($\kappa = 0$) show that it gives better accuracy than the uniform-grid integral equation methods. Hence, maintaining accuracy in this case would require implementing an adaptive mesh refinement scheme to fully take advantage of the reduced number of unknowns that the integral formulations afford.

Finally, Section 7 ventures briefly into the study of the initial-boundary value problem for the nonlinear evolution equation (1.1), and presents some numerical results based on the particle and integral equation methods, which can be adapted easily to the boundary value problem under the appropriate circumstances.

2. The integrable formulation and particle method

By introducing the characteristics $x = q(\xi,t)$,

$$\frac{\mathrm{d}q}{\mathrm{d}t} = u(q(\xi,t),t), \quad q(\xi,0) = \xi, \tag{2.1}$$

a solution of Eq. (1.1) follows formally from the Hamiltonian system:

$$\begin{aligned} q_t(\xi,t) &= \frac{1}{2}\int_{-\infty}^{\infty} \mathrm{e}^{-|q(\xi,t)-q(\eta,t)|}p(\eta,t)\,\mathrm{d}\eta - \kappa, \\ p_t(\xi,t) &= \frac{1}{2}\int_{-\infty}^{\infty} \operatorname{sgn}(\xi-\eta)\mathrm{e}^{-|q(\xi,t)-q(\eta,t)|}p(\xi,t)p(\eta,t)\,\mathrm{d}\eta. \end{aligned} \tag{2.2}$$

Here the characteristics $q(\xi,t)$ play the role of positions conjugate to the momentum-like variables $p(\xi,t)$ [4] in the Hamiltonian

$$H = \frac{1}{4}\int_{-\infty}^{\infty}\int_{-\infty}^{\infty} \left(\mathrm{e}^{-|q(\xi,t)-q(\eta,t)|}p(\eta,t)p(\xi,t) - \kappa(p(\xi,t)+p(\eta,t))\right)\mathrm{d}\eta\,\mathrm{d}\xi,$$

which yields system (2.2) by the (standard) Poisson structure,

$$q_t = \frac{\delta H}{\delta p}, \quad p_t = -\frac{\delta H}{\delta q},$$

with functional derivatives $\delta/\delta q$ and $\delta/\delta p$ with respect to the functions $q(\xi,t)$ and $p(\xi,t)$ at fixed time t. The choice of initial condition for the position variable, dictated by the characteristics condition, implies $q_\xi(\xi,0) = 1$, so that the constraint

$$q_\xi(\xi,t) = \frac{p(\xi,0)}{p(\xi,t)} \tag{2.3}$$

is maintained at all times of existence of the solution $(q(\xi,t),p(\xi,t))$. Thus, the momentum variable $p(\xi,t)$ could be eliminated from the system to obtain an evolution equation containing only the dependent variable $q(\xi,t)$ and its first derivative with respect to the initial label ξ. Vanishing of this derivative generically corresponds to crossing of characteristics curves, with loss of uniqueness of solutions $\xi(x)$ to the equation $x = q(\xi,\cdot)$. Constraint (2.3) then shows that if the initial condition $p(\xi,0)$ does not have zeros, $q_\xi(\cdot,t)$ is bounded away from zero, thereby preventing characteristics from crossing, for as long as $|p(\cdot,t)| < \infty$ [4]. The relation of system (2.2) with the original form (1.1) of the shallow-water wave equation results from the definition of the velocity $u(x,t)$ in terms of characteristics $q(\xi,t)$ and the conjugate momentum $p(\xi,t)$,

$$u(x,t) = -\kappa + \frac{1}{2}\int_{-\infty}^{\infty} \mathrm{e}^{-|x-q(\eta,t)|}p(\eta,t)\,\mathrm{d}\eta. \tag{2.4}$$

(In order for $u(x,t)$ to satisfy vanishing boundary conditions as $|x| \to \infty$, one must impose $p(\xi,t) \to \kappa$ sufficiently fast as $|\xi| \to \infty$; we will examine this decay condition, which can be controlled by the initial condition

$p(\xi,0)$, in more detail later on.) In fact, if characteristics do not cross, and $q(\cdot,t)$ is a monotonic function of ξ at all times $t<\infty$, then

$$u(x,t)-u_{xx}(x,t)=-\kappa+\int_{-\infty}^{\infty}\delta(x-q(\eta,t))p(\eta,t)\,\mathrm{d}\eta=-\kappa+\frac{p(\xi,t)}{q_\xi(\xi,t)}, \tag{2.5}$$

where ξ is such that $q(\xi,t)=x$ and we have used the fact that $\mathrm{e}^{-|x|}/2$ is the Green function for the operator $1-\partial_x^2$ (on the real line with vanishing boundary condition at infinity) together with the Dirac-δ identity,

$$\delta(f(x))=\sum_{k=1}^{M}\frac{1}{|f'(x_k)|}\delta(x-x_k),$$

valid for any C^1-function f with simple zeros at $x=x_k$. Moreover, the definition of characteristics (2.1), interpreted as a change of variables $\xi\to x$, and the definition (2.4) imply

$$u_x(x,t)=\left(\frac{1}{q_\xi}\frac{\partial}{\partial\xi}\right)u(q(\xi,t),t)=\frac{q_{\xi t}}{q_\xi}. \tag{2.6}$$

Eq. (1.1) assumes a particularly compact form [7] by defining the auxiliary field $m(x,t)$ as the right hand side of Eq. (2.5), or $m(x,t)\equiv(1-\partial_x^2)u(x,t)$. From (2.5), the constraint (2.3), and the identity (2.6), we obtain

$$\frac{\mathrm{d}m}{\mathrm{d}t}\equiv\frac{\partial}{\partial t}\left(\frac{p(\xi,t)}{q_\xi(\xi,t)}\right)=-2\frac{p(\xi,0)}{(q_\xi(\xi,t))^3}q_{\xi t}(\xi,t)=-2\frac{p(\xi,t)}{q_\xi(\xi,t)}\frac{q_{\xi t}(\xi,t)}{q_\xi(\xi,t)}=-2(m+\kappa)u_x,$$

or, eliminating the characteristics variables,

$$m_t+um_x=-2(m+\kappa)u_x. \tag{2.7}$$

This equation is equivalent to (1.1) once m is replaced by $u-u_{xx}$. Notice that the initial condition $q_\xi(\xi,0)=1$ and relation (2.5) imply $m_0(\xi)+\kappa=p(\xi,0)$, where $m_0(\cdot)$ is the initial value of $m(\cdot,t)$. Hence the constraint (2.3) can also read

$$p(\xi,t)=\frac{m_0(\xi)+\kappa}{q_\xi(\xi,t)}. \tag{2.8}$$

For the numerical algorithm to be developed later, it is convenient to put system (2.2) in a slightly different (but entirely equivalent) form:

$$q_t(\xi,t)=\frac{1}{2}\int_{-\infty}^{\infty}\mathrm{e}^{-|q(\xi,t)-q(\eta,t)|}\left(p(\eta,t)-\kappa\frac{\partial q}{\partial\eta}(\eta,t)\right)\mathrm{d}\eta, \tag{2.9a}$$

$$p_t(\xi,t)=\frac{1}{2}p(\xi,t)\int_{-\infty}^{\infty}\mathrm{sgn}(\xi-\eta)\mathrm{e}^{-|q(\xi,t)-q(\eta,t)|}\left(p(\eta,t)-\kappa\frac{\partial q}{\partial\eta}(\eta,t)\right)\mathrm{d}\eta, \tag{2.9b}$$

where we have used the properties of the kernel $\exp|x-y|$ to take the constant κ under the integral sign. The numerical algorithm proposed in [4] approximates the integrals in Eq. (2.2) by their Riemann sums, thereby yielding Hamiltonian systems for "particles" with coordinates

$$q_i(t)\equiv q(\xi_i,t)$$

and momenta

$$p_i(t)\equiv p(\xi_i,t),$$

where $\xi_i=\Xi+\mathrm{i}h$ for some real Ξ, step-size $h>0$ and $i=1,\ldots,b,N$.

By replacing q_η in system (2.9) by the constraint (2.3), the discretized version of this system results in the finite dimensional system of ODEs for N particles for Eq. (2.9):

$$\begin{aligned}\dot{q}_i&=\frac{h}{2}\sum_{j=1}^{N}\mathrm{e}^{-|q_i-q_j|}p_j-\frac{h}{2}\kappa\sum_{j=1}^{N}\mathrm{e}^{-|q_i-q_j|}p_j^0/p_j,\\ \dot{p}_i&=\frac{h}{2}p_i\sum_{i\neq j=1}^{N}\mathrm{sgn}(q_i-q_j)\mathrm{e}^{-|q_i-q_j|}p_j-\frac{h}{2}\kappa p_i\sum_{i\neq j=1}^{N}\mathrm{sgn}(q_i-q_j)\mathrm{e}^{-|q_i-q_j|}p_j^0/p_j,\end{aligned} \tag{2.10}$$

where $p(\xi_j,0)\equiv p_j^0$. We will refer to system (2.10) as *the particle method* for solving the shallow-water wave equation (1.1).

Remark 2.1. The compact form of the shallow-water wave equation (2.7) is reminiscent of the vorticity formulation for the incompressible Euler equations of an ideal fluid, with m in the role of vorticity. Thus, in Eq. (2.10) the conjugate pairs $\{q_i(t),p_i(t)\}$ play a role in the class of weak solutions of Eq. (1.1) [7]

$$u(x,t)=-\kappa+\sum_{j=1}^{N}p_j(t)\mathrm{e}^{-|x-q_j(t)|}, \tag{2.11}$$

analogous to that in the singular velocity solutions induced by point vortices for incompressible Euler equations [25].

Remark 2.2. Particle methods have been discussed in the context of evolution equations with similar structure, and in particular for dispersive wave equations, in [10]. While different from ours, the approach used therein can result in a similar system of ODEs. In addition to particle methods, examples of numerical integration schemes based on the characteristics formulation of an evolution equation have recently appeared in the literature [34].

Remark 2.3. It should be stressed that the (q,p) system is in principle more general than the shallow-water wave equation (1.1), which follows from system (2.2) as a particular case once the constraint (2.3) is taken into account. The constraint has the effect of removing one degree of freedom from the system, effectively projecting it to an invariant solution manifold where the dynamics is governed by Eq. (1.1) where only the first time-derivative appears. It is remarkable that system (2.2) itself follows from a more general class of systems which possess a Lax-pair, and hence it belongs to the family of completely integrable equations. It can be shown [4] that the isospectral problem:

$$\begin{aligned}\lambda\phi(\xi,t)&=\int_{-\infty}^{\infty}k(\xi,\eta;t)\phi(\eta,t)\,\mathrm{d}\eta,\\ \phi_t(\xi,t)&=\frac{1}{2}\int_{-\infty}^{\infty}\operatorname{sgn}(\xi-\eta)k(\xi,\eta;t)\phi(\eta,t)\,\mathrm{d}\eta\end{aligned} \tag{2.12}$$

yields system (2.2) for the special choice of the symmetric kernel $k(\xi,\eta;t)$ given in terms of $q(\xi,t)$ and (non-negative) $p(\xi,t)$ by

$$k(\xi,\eta;t)=\frac{1}{2}\mathrm{e}^{-\frac{1}{2}|q(\xi,t)-q(\eta,t)|}\sqrt{p(\xi,t)p(\eta,t)}. \tag{2.13}$$

2.1. Particle collisions

The numerical scheme based on the particle method relies on existence and uniqueness of solutions of the initial value problem for system (2.10). Moreover, collisions among particles are undesirable, and it might be expected that these correspond to finite-time singularities in the ODEs' solution. This section will examine these issues in some detail. For simplicity, let us consider the initial value problem for case $\kappa=0$ of the Hamiltonian system (2.10)

$$\dot{q}_i=\frac{1}{2}h\sum_{j=1}^{N}\mathrm{e}^{-|q_i-q_j|}p_j,\quad \dot{p}_i=\frac{1}{2}h\sum_{i\neq j=1}^{N}\operatorname{sgn}(q_i-q_j)\mathrm{e}^{-|q_i-q_j|}p_ip_j. \tag{2.14}$$

The initial values of interest for the q-variables inherently define an ordering $q_1^0<q_2^0\cdots<q_N^0$ of the initial values for the vector q. (Henceforth, with a slight abuse of notation, no-subscript letters will denote $\mathbb{R}^N$-vectors, with their $\mathbb{R}^N$-norm represented by $\|\cdot\|$.) In fact, as remarked above, for the initial grid in the particle method one takes $q_i^0=\Xi+\mathrm{i}h,\ i=1,\ldots,N$.

Existence for any finite N of the solution $\{q_i(t),p_i(t)\}_{i=1}^N$ can then be established globally in time by the following propositions, provided the data for the p-variables are appropriately chosen:

Proposition 2.1. *The vector field of system* (2.10) *is Lipschitz continuous on* $(q,p) \in D$, *where* $D \subset \mathbb{R}^{2N}$ *is the finite subset*

$$-\infty < l_m < q_1 < q_2 \cdots < q_N < l_M < \infty, \quad \|p\| < l_p < \infty.$$

Proof. We first establish Lipschitz-continuity of the first N components (the $\dot{q}$-part) of system (2.10) on D. For *any* two pairs of vectors $(q,p) \in \mathbb{R}^{2N}$, $(\tilde{q},\tilde{p}) \in \mathbb{R}^{2N}$,

$$\begin{aligned}
\left|\frac{h}{2}\sum_{j=1}^{N} \mathrm{e}^{-|\tilde{q}_i-\tilde{q}_j|}\tilde{p}_j - \frac{h}{2}\sum_{j=1}^{N} \mathrm{e}^{-|q_i-q_j|}p_j\right| &\leqslant \frac{h}{2}\sum_{j=1}^{N} |\mathrm{e}^{-|\tilde{q}_i-\tilde{q}_j|}\tilde{p}_j - \mathrm{e}^{-|q_i-q_j|}\tilde{p}_j + \mathrm{e}^{-|q_i-q_j|}\tilde{p}_j - \mathrm{e}^{-|q_i-q_j|}p_j| \\
&\leqslant \frac{h}{2}\sum_{j=1}^{N} \left(\left|\mathrm{e}^{-|\tilde{q}_i-\tilde{q}_j|} - \mathrm{e}^{-|q_i-q_j|}\right||\tilde{p}_j| + |\tilde{p}_j - p_j|\right) \\
&\leqslant \frac{h}{2}|\tilde{p}|_{\max}\left(\sum_{j=1}^{N} \left||\tilde{q}_i-\tilde{q}_j| - |q_i-q_j|\right|\right) + \frac{h}{2}\sum_{j=1}^{N}|\tilde{p}_j - p_j| \\
&\leqslant \frac{h}{2}\|\tilde{p}\|\left(N|\tilde{q}_i - q_i| + \sum_{j=1}^{N}|\tilde{q}_j - q_j|\right) + \frac{h}{2}\|\tilde{p}-p\|, \qquad (2.15)
\end{aligned}$$

where by $\|\cdot\|$ we have denoted the 1-norm $\|r\| \equiv \sum_{j=1}^{N}|r_j|$ and we have used the inequality

$$|\mathrm{e}^{-a} - \mathrm{e}^{-b}| \leqslant \mathrm{e}^{-\inf(a,b)}|a-b|$$

valid for any two non-negative reals a and b. The last inequality in (2.15) allows us to conclude that

$$\|F^{(q)}(q,p) - F^{(q)}(\tilde{q},\tilde{p})\| \leqslant L^{(q)}(\|q-\tilde{q}\| + \|p-\tilde{p}\|),$$

where by $F^{(q)}(q,p) \in \mathbb{R}^N$ we have denoted the vector field of the first N components of system (2.10), and the Lipschitz constant $L^{(q)}$ is

$$L^{(q)} = \frac{Nh}{2}\sup(2l_p, 1).$$

This establishes Lipschitz-continuity for the first N components of the vector field (2.10) in the ball D. For the other N components (the $\dot{p}$-part of the system) we proceed similarly estimate (2.15), and use the ordering assumption to factor $\mathrm{sgn}(\tilde{q}_i - \tilde{q}_j) = \mathrm{sgn}(q_i - q_j)$:

$$\begin{aligned}
&\left|\frac{h}{2}\sum_{j=1}^{N} \mathrm{sgn}(\tilde{q}_i-\tilde{q}_j)\mathrm{e}^{-|\tilde{q}_i-\tilde{q}_j|}\tilde{p}_i\tilde{p}_j - \frac{h}{2}\sum_{j=1}^{N} \mathrm{sgn}(q_i-q_j)\mathrm{e}^{-|q_i-q_j|}p_ip_j\right| \\
&\leqslant \frac{h}{2}\sum_{j=1}^{N} |\mathrm{e}^{-|\tilde{q}_i-\tilde{q}_j|}\tilde{p}_i\tilde{p}_j - \mathrm{e}^{-|q_i-q_j|}\tilde{p}_ip_j + \mathrm{e}^{-|q_i-q_j|}\tilde{p}_ip_j - \mathrm{e}^{-|q_i-q_j|}p_ip_j| \\
&\leqslant \frac{h}{2}\sum_{j=1}^{N} \left(\left|\mathrm{e}^{-|\tilde{q}_i-\tilde{q}_j|}\tilde{p}_j - \mathrm{e}^{-|q_i-q_j|}p_j\right||\tilde{p}_i| + |\tilde{p}_i - p_i||p_j|\right) \\
&\leqslant \frac{h}{2}l_p\left(Nl_p|\tilde{q}_i - q_i| + l_p\sum_{j=1}^{N}|\tilde{q}_j - q_j| + \|\tilde{p}-p\| + N|\tilde{p}_i - p_i|\right), \qquad (2.16)
\end{aligned}$$

where we have used the estimate established by (2.15) to produce the first three terms in the last inequality. This establishes Lipschitz continuity for the other p-components of the vector field (2.10) in the ball D,

$$\|F^{(p)}(q,p) - F^{(p)}(\tilde{q},\tilde{p})\| \leqslant L^{(p)}(\|q-\tilde{q}\| + \|p-\tilde{p}\|),$$

with Lipschitz constant

$$L^{(p)} = Nhl_p\sup(l_p, 1). \quad \square$$

Local existence in time follows immediately by this Proposition, by the standard theorems for ODE systems [12], so that we have also proved:

Proposition 2.2. *Consider the initial value problem for system* (2.10) *with initial condition* $\{q_i(0), p_i(0)\}_{i=1}^N = \{q_i^0, p_i^0\}_{i=1}^N \in \mathbb{R}^{2N}$, *where the q components are assumed to be ordered,* $q_1^0 < q_2^0 \cdots < q_N^0$, *and*

$$\inf_{i\neq j}(|q_i^0 - q_j^0|) \geqslant \delta > 0.$$

Let D be the subset of $\mathbb{R}^{2N}$ *such that* $|q_i - q_i^0| > 0$, $i = 1,\ldots,N$, *and* $\|p - p^0\| < l_p$. *A unique solution exists for* $0 \leqslant t < T_e$, *where* $T_e \leqslant \inf(\delta/(2M^{(q)}), l_p/M^{(p)})$, *with* $M^{(q)} \equiv \sup_D\|F^{(q)}\|$ *and* $M^{(p)} \equiv \sup_D\|F^{(p)}\|$.

When system (2.14) is viewed as a particle method to solve the original PDE (1.1), the minimum distance δ between initial qs in this proposition simply coincides with the discretization step h. Because of this, the time T_e of existence guaranteed by Proposition 2.2 could be too small to serve any practical purpose. However, we can extend existence to all times by an appropriate definition of the initial data. The above local existence result does not make use of the Hamiltonian nature of system (2.14), nor of its complete integrability. In order to establish global existence in time, we will make use of both properties. While this may be overkill, it is effective in dealing with global properties of the system. The following proposition establishes global existence by restricting the initial data for the momenta to be strictly positive. This has the effect of maintaining the (strict) ordering of the position variables, which in turn keeps the solution within the Lipschitz domain.

Proposition 2.3. *If the initial momenta are positive,* $p_i \geqslant \epsilon > 0$, $i = 1,\ldots,N$ *for some constant* ϵ, *then the solution of system* (2.14) *exists uniquely for all times, or* $T_e = \infty$. *In particular, no two particles can occupy the same position* $q_i(t) = q_j(t)$, *for some* $i \neq j$, *at any finite time t.*

Proof. We first notice that translation invariance $q \to q + r$ for any constant vector $r \in \mathbb{R}^N$ of the Hamiltonian system (2.14) suggests that some version of total momentum should be conserved. It is easy to see that P defined by

$$P = \frac{1}{2}h\sum_{i=1}^{N} p_i \tag{2.17}$$

is invariant in time, by summing the $\dot{p}$ equation and using the antisymmetry of the sums for exchange of indexes. If all the initial momenta are positive, then for as long as the momenta remain positive, which by C^1-continuity with respect to t has to hold for some time $t < T_s \leqslant T_e$, Gronwall inequality yields

$$-Pt + \log(p_i(0)) \leqslant \log(p_i(t)) \leqslant Pt + \log(p_i(0))$$

or

$$p_i(0)e^{-Pt} \leqslant p_i(t) \leqslant p_i(0)e^{Pt}. \tag{2.18}$$

Now extending T_s, one can see that the left inequality prevents $p_i(t)$ for all $i = 1,\ldots,N$ from changing sign through a zero crossing, while the right inequality prevents a change in sign through infinity, for all times $t < \infty$. Going back to the qs, the velocities and positions are bounded by P and $Pt + q_i^0$, $t < \infty$, respectively. Thus, the switching-sign time T_s is larger than the existence time T_e. The bound (2.18) shows that the minimum time for the p-components of the solution to reach the boundary of the Lipschitz domain D can be extended to be arbitrarily large by increasing l_p. A continuation argument can now be used to extend T_e to infinity, since the only way for the solution to leave the Lipschitz domain D in finite time is through a loss of ordering of the position variables qs.

Because of the bounds on the magnitude of the qs, extending T_e to infinity is thus equivalent to showing that no particle collision can occur, or $q_i(T_c) = q_j(T_c)$ for some $i \neq j$, and some finite time T_c. This of course has the implication that the qs relative initial ordering cannot be changed in the course of the evolution. For this, it is advantageous to use the complete integrability of system (2.14). First, notice that this system can be obtained [4] from the compatibility condition (the Lax pair inherited from system (2.12)) between

$$\lambda\varphi_i(t) = h\sum_j^N k_{ij}(t)\varphi_j(t), \quad \dot{\varphi}_i(t) = \frac{1}{2}h\sum_{j=1}^{i-1} k_{ij}(t)\varphi_j(t) - \frac{1}{2}h\sum_{j=i+1}^{N} k_{ij}(t)\varphi_j(t), \tag{2.19}$$

where $k_{ij}(t)$ are the (i,j)-entries of a symmetric matrix, K say, defined by

$$k_{ij}(t) = \frac{1}{2}\mathrm{e}^{-\frac{1}{2}|q_i(t)-q_j(t)|}\sqrt{p_i(t)p_j(t)}. \tag{2.20}$$

If the spectrum of the matrix K is constant in time system (2.19) implies the evolution of q,p (2.14), as taking the time derivative of first equation and multiplication by λ of second one in (2.19) readily shows. Conversely, if q,p evolve in time according to (2.14), then this system implies that the spectrum is constant in time, in particular $\det K(t) = \det K(0)$.

Because the matrix K can be factorized as

$$K = SES,$$

where

$$[S]_{ij} = \sqrt{p_j}\delta_{ij}, \quad [E]_{ij} \equiv e_{ij} = \exp(|q_i(t) - q_j(t)|/2),$$

the determinant of K is given by the product of the eigenvalues λ_i, $i = 1,\ldots,N$, and

$$\det K = \prod_{i=1}^{N}\lambda_i = \text{const.} = \left(\prod_{i=1}^{N} p_i\right)\det E.$$

Thus, for our purposes it is sufficient to focus on the symmetric matrix E. If, in fact, $\det E$ were to vanish, then the p-product would have to diverge in order for $\det K$ to be constant.

The determinant can be written as

$$\sum_{\mathscr{P}} \varepsilon^{i_1,i_2,\ldots,i_N} e_{1i_1}e_{2i_2}\cdots e_{Ni_N},$$

where the sums are taken over all the permutations $\mathscr{P}$ of the integers $i_1,i_2,\ldots,i_N$, and $\varepsilon^{i_1,i_2,\ldots,i_N}$ is the Levi–Civita completely antisymmetric tensor of order N.

We argue by contradiction. Suppose that there exists time $t = T_c$ at which two particles coincide, say the jth and the kth, and $j < k$. Then, the two factors e_{ji_j} and e_{ki_k} in the sum's generic term become e_{ji_j} and e_{ji_k}, and so

$$e_{1i_1}\cdots e_{ji_j}\cdots e_{ki_k}\cdots e_{N,i_N} = e_{1i_1}\cdots e_{ji_j}\cdots e_{ji_k}\cdots e_{N,i_N} = e_{1i_1}\cdots e_{ji_k}\cdots e_{ji_j}\cdots e_{N,i_N}.$$

The indexes $i_1,i_2,\ldots,i_N$ are dummy indexes of summation. We can therefore write

$$\begin{aligned}\sum_{\mathscr{P}} \varepsilon^{i_1,i_2,\ldots,i_j,\ldots,i_k,\ldots,i_N} e_{1i_1}\cdots e_{ji_j}\cdots e_{ji_k}\cdots e_{N,i_N} &= \sum_{\mathscr{P}} \varepsilon^{i_1,i_2,\ldots,i_j,\ldots,i_k,\ldots,i_N} e_{1i_1}\cdots e_{ji_k}\cdots e_{ji_j}\cdots e_{N,i_N} \\ &= \sum_{\mathscr{P}} \varepsilon^{i_1,i_2,\ldots,i_k,\ldots,i_j,\ldots,i_N} e_{1i_1}\cdots e_{ji_j}\cdots e_{ji_k}\cdots e_{N,i_N}.\end{aligned} \tag{2.21}$$

We can return the indexes i_j and i_k to their original positions in the tensor ε by permutations. With $k-j$ "hops" the index i_j can be brought in front of i_k in the last sum in (2.21). The index i_k can then be returned to its original slot by $k-j-1$ hops. The total number of permutations is therefore $2(k-j)-1$, which implies, by the antisymmetry of $\varepsilon^{i_1,i_2,\ldots,i_N}$

$$\sum_{\mathscr{P}} \varepsilon^{i_1,i_2,\ldots,i_j,\ldots,i_k,\ldots,i_N} e_{1i_1}\cdots e_{ji_j}\cdots e_{ji_k}\cdots e_{N,i_N} = -\sum_{\mathscr{P}} \varepsilon^{i_1,i_2,\ldots,i_j,\ldots,i_k,\ldots,i_N} e_{1i_1}\cdots e_{ji_j}\cdots e_{ji_k}\cdots e_{N,i_N}$$

or

$$\det E = -\det E$$

and so $\det E = 0$ if $q_j(T_c) = q_k(T_c)$. Hence, if two particles collide at time T_c, i.e., $q_j(t) \to q_k(t)$ as $t \uparrow T_c$, then $\det S \to \infty$ in the same limit, which contradicts the bound on each individual p_i, $i = 1,\ldots,N$, established by (2.18). We conclude that any two particles in the set cannot occupy the same location at any finite time, if the initial momenta of all particles are chosen to be positive so that estimate (2.18) holds, that is, the collision

time T_c is larger than the existence time T_e. Hence, any finite existence time T_e cannot be maximal and the solution $(q(t),p(t))$ can be continued for all finite times $t < \infty$. □

Remark 2.4. The global existence result can easily be modified to include the case $\kappa \neq 0$, as it is evident from the integrable formulation (2.2), which shows that the p-components are simply shifted by the constant κ. In this case the restriction to positive initial momenta corresponds to $m_0(x) + \kappa > 0$ by definition (2.8), which has a natural physical interpretation for the class of initial conditions consistent with the asymptotic derivation of the shallow-water wave model (1.1). Also worth noticing is that while collisions lead to the blow-up of the solution in the momentum components, it is possible to continue the solution past blow-up time(s) by defining an appropriate set of rules, such as energy conservation, using the dynamical system structure of the ODEs [7].

Remark 2.5. For fixed h, the system of ODE (2.14) and its more general form (2.10) are members of the (extended) Toda-lattice family [27,23,26]. This connection becomes particularly transparent when viewed from the Lax-pair (2.19) [4], but, as mentioned above, the complete integrability of the system needs further study in order to be used for addressing issues of practical relevance for the continuum (PDE) solutions of (1.1), as we will see in later sections.

3. Convergence of the particle method

In [4] several test problems, including the case of a travelling wave, presented numerical evidence for the convergence of the particle algorithm. Our efforts in this and the following sections are devoted to proving convergence of the particle method (2.10), and further to providing a fast summation algorithm for this method which reduces the computational cost from the original order $O(N^2)$ to order $O(N)$, where N is the number of particles.

Our proof of convergence of the particle method will focus on the case $\kappa = 0$ (similarly to our approach in the previous section), since it is then straightforward to extend the proof to the case $\kappa \neq 0$.

Let $q(\xi,t)$, $p(\xi,t)$ denote the solution to the continuous problem (2.9) corresponding to the initial data

$$q(\xi,0) = \xi, \quad p(\xi,0) = p^0(\xi), \tag{3.1}$$

while $\tilde{q}(t)$, $\tilde{p}(t)$ will stand for the solution of the particle system (2.14) emanating from initial conditions

$$\tilde{q}_i(0) = q(\xi_i,0) \equiv \xi_i, \quad \tilde{p}_i(0) = p^0(\xi_i). \tag{3.2}$$

Let $q_i(t) = q(\xi_i,t)$ denote the PDE solution evaluated at the grid points, and define the difference between PDE and ODE variables as

$$\phi_i = q_i - \tilde{q}_i, \quad \psi_i = p_i - \tilde{p}_i. \tag{3.3}$$

In what follows, we will work with the (discrete) l_1-norm, defined by

$$\|\phi\| = h \sum_j |\phi_j|. \tag{3.4}$$

Let the initial total momentum $P < \infty$ be defined as in Eq. (2.17). We have the following convergence theorem:

Theorem 3.1. *Consider the initial value problems* (3.1) *and* (3.2) *for systems* (2.9) *and* (2.14), *respectively*, *with* $\kappa = 0$. *If the function* $p^0(\xi) > 0$ *is sufficiently smooth and decays rapidly at infinity*, *for any finite time* $T > 0$ *there exists a grid-step size h such that the difference between the continuum and discrete variable satisfies*

$$\|\phi\| + \frac{1}{P}\|\psi\| \leqslant h^2 \frac{C}{2LP}(e^{2LPt} - 1) \tag{3.5}$$

for $0 \leqslant t < T$, *where C is a constant independent of T or h and* $L > \frac{1+h/2}{2}$.

Proof. (Here and unless explicitly mentioned in all the following, we will use the convention that the particle index ranges from $-N/2$ to $N/2$, so that the actual particle number is $N+1$.)

Consistency – the error estimate between the particle method solution and that of the integrable system takes form

$$|\tilde{q}_i(t) - q(\xi_i,t)| \leqslant \int_0^t \left| \frac{h}{2} \sum_{j=-N/2}^{N/2} \mathrm{e}^{-|q_i(s)-q_j(s)|} p_j(s) - \frac{1}{2} \int_{-\infty}^{\infty} \mathrm{e}^{-|q(\xi,s)-q(\eta,s)|} p(\eta,s)\,\mathrm{d}\eta \right| \mathrm{d}s$$
$$+ \int_0^t \left| \frac{h}{2} \sum_{j=-N/2}^{N/2} \mathrm{e}^{-|\tilde{q}_i(s)-\tilde{q}_j(s)|} \tilde{p}_j(s) - \frac{h}{2} \sum_{j=-N/2}^{N/2} \mathrm{e}^{-|q_i(s)-q_j(s)|} p_j(s) \right| \mathrm{d}s, \tag{3.6}$$

where we have used the initial conditions $\tilde{q}_i(0) = q_i(\xi_i,0) = \xi_i$. The first term of the right hand side is usually referred to as the consistency error and measures the error due to the replacement of the continuous problem by a finite discretization. The momentum-like variable $p(\xi,t)$ is defined in (2.8), and so it is bounded as long as $0 < q_\xi(\xi,t) < \infty$. In particular, if $m_0(\xi)$ is in the Schwartz class, the initial condition implies $q_\xi(\xi,0) = 1$ and so $p(\xi,0)$ is in the Schwartz class. It follows that $p(\xi,t)$ is in the Schwartz class as long as $q_\xi(\xi,t)$ is away from zero. It is shown in [4] that $q_\xi(\xi,t) \neq 0$ for any finite period of time, if $m_0(\xi)$ is non-negative. Thus $p(\xi,t)$ is also in the Schwartz class for any time $t < T < \infty$. (When $\kappa \neq 0$, this conclusion applies to the difference $p(\xi,t) - \kappa$.) Hence there exists a finite integer N and a domain $[-d_N,d_N]$ such that integral "tails" outside the domain are estimated by

$$\int_{-\infty}^{-d_N} \mathrm{e}^{-|q(\xi,t)-q(\eta,t)|} p(\eta,t)\,\mathrm{d}\eta = \mathrm{O}(\mathrm{e}^{-cN}), \quad \int_{d_N}^{\infty} \mathrm{e}^{-|q(\xi,t)-q(\eta,t)|} p(\eta,t)\,\mathrm{d}\eta = \mathrm{O}(\mathrm{e}^{-cN}) \tag{3.7}$$

for some constant $c > 0$ and increasing N, d_N. With these estimates, the approximation of the definite integral

$$\int_{-d_N}^{d_N} \mathrm{e}^{-|q(\xi,t)-q(\eta,t)|} p(\eta,t)\,\mathrm{d}\eta$$

by its Riemann sum is equivalent to the composite trapezoidal rule. In particular, the integrand $\mathrm{e}^{-|q(\xi,t)\,-\,q(\eta,t)|} p(\eta,t)$ is smooth on the domain except at one point. Thus the consistency error is $\mathrm{O}(h^2)$ globally on the domain, if the discontinuity generated by $\mathrm{sgn}(q(\xi,t) - q(\eta,t))$ is aligned with the grid. The property of non-crossing of characteristics [4] implies $\mathrm{sgn}(q(\xi,t) - q(\eta,t)) = \mathrm{sgn}(\xi - \eta)$ for all finite times (if the initial momentum $p_\xi(\xi,0) > 0$). This implies that the initial grid remains aligned with the discontinuities of the integrand at all times, provided it is so initially. We conclude that the consistency error for the q- and p-differences is $\mathrm{O}(h^2)$ globally for any finite time. (We remark that, as seen from the above considerations, the dispersive case $\kappa \neq 0$ is treated on equal footing as the non-dispersive case $\kappa = 0$, and the consistency error is quadratic regardless of the choice of κ.)

Stability: the second term of the right hand side of estimate (3.6) represents the stability error and measures the error due to summing over approximate particle positions rather than the exact ones. By the non-crossing property of particles for both the continuum and discretized systems, one arrives at the following estimate (using manipulations similar to those of the Lipschitz continuity proof in Section 2.1):

$$\left| \frac{h}{2} \sum_{j=-N/2}^{N/2} \mathrm{e}^{-|\tilde{q}_i-\tilde{q}_j|} \tilde{p}_j - \frac{h}{2} \sum_{j=-N/2}^{N/2} \mathrm{e}^{-|q_i-q_j|} p_j \right| \leqslant \frac{h}{2} \sum_{j=-N/2}^{N/2} |\mathrm{e}^{-|\tilde{q}_i-\tilde{q}_j|} \tilde{p}_j - \mathrm{e}^{-|q_i-q_j|} \tilde{p}_j + \mathrm{e}^{-|q_i-q_j|} \tilde{p}_j - \mathrm{e}^{-|q_i-q_j|} p_j|$$
$$\leqslant \frac{h}{2} \sum_{j=-N/2}^{N/2} \left(P \left| \mathrm{e}^{-|\tilde{q}_i-\tilde{q}_j|} - \mathrm{e}^{-|q_i-q_j|} \right| + |\tilde{p}_j - p_j| \right) \tag{3.8}$$

and so,

$$\left| \frac{h}{2} \sum_{j=-N/2}^{N/2} \mathrm{e}^{-|\tilde{q}_i-\tilde{q}_j|} \tilde{p}_j - \frac{h}{2} \sum_{j=-N/2}^{N/2} \mathrm{e}^{-|q_i-q_j|} p_j \right|$$
$$\leqslant \frac{h}{2} P \left(\sum_{j=-N/2}^{i-1} |\mathrm{e}^{-(\tilde{q}_i-\tilde{q}_j)}||1 - \mathrm{e}^{(\tilde{q}_i-\tilde{q}_j)-(q_i-q_j)}| + \sum_{j=i}^{N/2} \left|\mathrm{e}^{-(q_j-q_i)}\right||1 - \mathrm{e}^{(q_j-q_i)-(\tilde{q}_j-\tilde{q}_i)}| \right) + \frac{h}{2} \sum_{j=-N/2}^{N/2} |\tilde{p}_j - p_j|$$
$$\leqslant \frac{h}{2} P \sum_{j=-N/2}^{N/2} |1 - \mathrm{e}^{-(q_i-\tilde{q}_i)+(q_j-\tilde{q}_j)}| + \frac{h}{2} \sum_{j=-N/2}^{N/2} |\tilde{p}_j - p_j|, \tag{3.9}$$

since the sum of total momenta is conserved and $P > p_i$ for all is at all times. Using the notation in Eq. (3.3), the inequality (3.6) takes the form

$$|\phi_i| \leqslant \int_0^t \left(\frac{h}{2} P \sum_j |1 - \mathrm{e}^{-\phi_i(s)+\phi_j(s)}| + \frac{h}{2} \sum_j |\psi_j(s)| \right) \mathrm{d}s + C_1 h^2 t, \tag{3.10}$$

where C_1 is some constant independent of t or h.

Similarly for the momentum $p(\xi,t)$, the error estimate also has two parts. We have argued that the consistency error is $O(h^2)$ globally on the domain. Since the stability error for the p part of the solution can be derived in a similar fashion to (3.9), we only present the final result omitting the details. The error estimate for the momentum can be written as

$$|\psi_i| \leqslant \int_0^t \left(\frac{h}{2} P^2 \sum_j |1 - \mathrm{e}^{-\phi_i(s)+\phi_j(s)}| + \frac{h}{2} P \sum_j |\psi_j(s)| + \frac{h}{2} P |\psi_i(s)| \right) \mathrm{d}s + C_2 h^2 t. \tag{3.11}$$

Since the function e^{ϕ} satisfies a Lipschitz condition, there exists an $L > 0$ such that

$$|1 - \mathrm{e}^{-\phi_i+\phi_j}| = \mathrm{e}^{-\phi_i} |\mathrm{e}^{\phi_i} - \mathrm{e}^{\phi_j}| \leqslant L|\phi_i - \phi_j| \leqslant L(|\phi_i| + |\phi_j|). \tag{3.12}$$

Equipped with the l_1-norm and the estimate (3.12), the error bounds (3.10) and (3.11) become:

$$\begin{aligned} \|\phi\| &\leqslant \int_0^t \left(LP\|\phi\| + \frac{1}{2}\|\psi\| \right) \mathrm{d}s + C_1 h^2 t, \\ \|\psi\| &\leqslant \int_0^t \left(LP^2\|\phi\| + \frac{P}{2}\|\psi\| + \frac{h}{2} P \|\psi\| \right) \mathrm{d}s + C_2 h^2 t. \end{aligned} \tag{3.13}$$

It follows that

$$\begin{aligned} \|\phi\| + \frac{1}{P}\|\psi\| &\leqslant \int_0^t \left(2LP\|\phi\| + \|\psi\| + \frac{h}{2}\|\psi\| \right) \mathrm{d}s + Ch^2 t \\ &\leqslant \int_0^t \left(2LP\left(\|\phi\| + \frac{1}{P}\|\psi\| \right) - \left(2L - \left(1 + \frac{h}{2} \right) \right) \|\psi\| \right) \mathrm{d}s + Ch^2 t \\ &\leqslant \int_0^t 2LP\left(\|\phi\| + \frac{1}{P}\|\psi\| \right) \mathrm{d}s + Ch^2 t, \end{aligned} \tag{3.14}$$

provided the Lipschitz constant $L > \frac{1+h/2}{2}$. Here C is a constant independent of t or h. We complete our proof by applying the Gronwall lemma [29]

$$\|\phi\| + \frac{1}{P}\|\psi\| \leqslant \frac{Ch^2}{2LP}(\mathrm{e}^{2LPt} - 1) \tag{3.15}$$

for $0 < t < T$.

The error due to a temporal discretization is not considered in the proof – the system of ODEs is assumed to be solved exactly. □

Besides convergence, estimate (3.15) shows that the particle method can be expected to be second order accurate. Notice that the accuracy could be improved with little extra effort by introducing local corrections to the standard trapezoidal rule (cf. Section 6.2 below).

4. Fast summation algorithm

The major computational cost for solving the system of $2N$ equations (2.10) is the cost of evaluating the Riemann sum at each time step. Computing the summations alone takes $O(N^2)$ operations for an N-particle system, if no recursion formulas are used.

In this section we propose a recursion formula based on the property discussed in Section 2.1 on the absence of particle collisions for finite times. This principle allows us to strip the absolute value notation in

the power of the exponential function, which in turn makes a recursion relation for evaluating the sums possible. With the help of this recursion formula, the total operations needed for performing the summation is reduced to O(N) for the N-particle system. We present the fast summation algorithm for the non-dispersive case $\kappa = 0$. The case $\kappa \neq 0$ is completely analogous but leads to longer expressions.

By the no-collision property, the particle method (2.10) has $q_i > q_j$ if $i > j$ and vice-versa if $i < j$. Hence Eq. (2.10) can be written as:

$$\begin{aligned} \dot{q}_i &= \frac{h}{2}\left(\sum_{j=1}^{i-1} \mathrm{e}^{-(q_i-q_j)}p_j + p_i + \sum_{j=i+1}^{N} \mathrm{e}^{-(q_j-q_i)}p_j\right), \\ \dot{p}_i &= \frac{h}{2}p_i\left(\sum_{j=1}^{i-1} \mathrm{e}^{-(q_i-q_j)}p_j - \sum_{j=i+1}^{N} \mathrm{e}^{-(q_j-q_i)}p_j\right). \end{aligned} \tag{4.1}$$

Define new variables:

$$\begin{aligned} f_i^l &= \sum_{j=1}^{i-1} \mathrm{e}^{-(q_i-q_j)}p_j, \\ f_i^r &= \sum_{j=i+1}^{N} \mathrm{e}^{-(q_j-q_i)}p_j. \end{aligned} \tag{4.2}$$

Eq. (4.1) then becomes:

$$\begin{aligned} \dot{q}_i &= \frac{h}{2}(f_i^l + p_i + f_i^r), \\ \dot{p}_i &= \frac{h}{2}p_i(f_i^l - f_i^r). \end{aligned} \tag{4.3}$$

One can see that with a pre-computed f^l and f^r the number of operations needed for the Riemann sum is O(N) for the $N \times N$ system of equations. Since the operations required for f^l or f^r are also growing as O(N), the total number of operations is O(N).

We now establish the recursion relation for f^l and f^r

$$\begin{aligned} f_{i+1}^l &= \sum_{j=1}^{i} \mathrm{e}^{-(q_{i+1}-q_j)}p_j = \sum_{j=1}^{i-1} \mathrm{e}^{-(q_{i+1}-q_j)}p_j + \mathrm{e}^{-(q_{i+1}-q_i)}p_i = \sum_{j=1}^{i-1} \mathrm{e}^{-(q_{i+1}-q_i)-(q_i-q_j)}p_j + \mathrm{e}^{-(q_{i+1}-q_i)}p_i \\ &= \mathrm{e}^{-(q_{i+1}-q_i)}\left(\sum_{j=1}^{i-1} \mathrm{e}^{-(q_i-q_j)}p_j + p_i\right) = \mathrm{e}^{-(q_{i+1}-q_i)}(f_i^l + p_i). \end{aligned} \tag{4.4}$$

Similarly,

$$f_{i+1}^r = \mathrm{e}^{-(q_i-q_{i+1})}f_i^r - p_{i+1}. \tag{4.5}$$

Because $\mathrm{e}^{-(q_i-q_{i+1})}$ leads to exponential growth, for numerical stability the recursion relation for f^r is better solved backward as

$$f_i^r = (f_{i+1}^r + p_{i+1})\mathrm{e}^{-(q_{i+1}-q_i)}. \tag{4.6}$$

We remark that for higher dimensions, the counterparts of the (double) exponential Green's function $\mathrm{e}^{-|x|}$ in one dimension, are, respectively, the modified Bessel function of order zero $K_0(|\vec{x}|)$ in 2D and $\mathrm{e}^{-k|\vec{x}|}/|\vec{x}|$ in 3D, i.e., the Green's functions for the modified Helmholtz equation $\Delta u(\vec{x}) - u(\vec{x}) = 0$. The efficient calculation of the ensuing convolutions can be carried out using the fast multipole methods (FMMs) introduced in [9,20].

5. Numerical results

This section presents two examples of application of the particle method to the numerical solution of Eq. (1.1). The first example tests the method on a traveling wave solution for the dispersive case $\kappa \neq 0$. The other

example deals with initial value problem of the non-dispersive case, $\kappa = 0$. The aim is to illustrate the efficiency and the order of accuracy for the scheme. For both cases (trivially when the initial condition corresponds to that of a smooth traveling wave solution) it may be expected that the solution evolves free of shocks for all times (a priori bounds on the initial condition [7] which ensure that a vertical slope is achieved in finite time at inflection points are violated for the initial conditions we consider). Nevertheless, for the dispersionless case $\kappa = 0$ the numerical simulation shows that a rather sharply peaked solitary wave forms and moves away from the origin. From the viewpoint of the particle method, the peaked solution arises from particles clustering rapidly in the region of the peak of the solitary wave(s). Such clustering behavior causes problems in the particle method, as the ordering of the particles becomes affected by numerical errors. An efficient implementation is introduced in this section to remove such complication.

5.1. Smooth travelling wave solution $\kappa \neq 0$

An *explicit* exact solution of Eq. (1.1) is $u(x,t) = U(x - ct) \equiv U(s)$ [6], where $c = 8\kappa/3$ and $U(s)$ is given by

$$U(s) = \frac{8}{3}\kappa\left(1 - \frac{3\sqrt{3} + 6\sin 2z}{(1 + 2\cos 2z)(2\sqrt{3}\cos 2z - \sqrt{3}\cos 4z + 2\sin 2z + \sin 4z)}\right) \tag{5.1}$$

with $z = \arctan(e^{s/2})/3$. The initial condition $u_0(x) = U(x)$ yields the initial data for the particle algorithm $q(x,0) = x$ and $p(x,0) = \kappa + m_0(x)$, where

$$m_0(x) = \kappa\left(\frac{c^2}{(c - U(x))^2} - 1\right). \tag{5.2}$$

With the initial condition (5.2), we compare the numerical solution computed by the particle method with the exact travelling wave solution to illustrate the order of convergence of the method.

We remark that a fixed ratio $\Delta t/h = 1/2$ is used for all calculations throughout this paper. This fixed ratio is for the purpose of numerical convergence tests. We chose the temporal discretization to be compliant with the choice of h used in the Riemann sum for the ODE system (2.10). Based on our experiments, we found that $\Delta t = h/2$ would suffice for all simulations in this paper to prevent the onset of numerical instability.

For the travelling wave simulation we take the constant $\kappa = 1$. The time integration proceeds through an explicit fourth-order Runge–Kutta method.

As indicated in (2.11), using the ps and qs obtained from the ODE system, the numerical solution for the PDE is then constructed on the physical domain. We study the numerical error between exact and computed solutions with the (finite) l_2-norm

$$\|\epsilon\| = \sqrt{\Delta x \sum_{j=1}^{\bar{N}} |u_{j,\text{exact}} - u_j|^2} = \sqrt{\Delta x \sum_{j=1}^{\bar{N}} \epsilon_j^2}, \tag{5.3}$$

where Δx is the grid size for the mesh on the physical domain, defined as $\Delta x = \bar{L}/\bar{N}$, with $\bar{L}$ the length of the physical domain and $\bar{N}$ is the number of grid points for this mesh. This Δx is independent of the increment h used in the Riemann sum for the ODE system, which is defined as $h = \Delta\eta = L/N$, where N is the number of particles and L is the length of the domain for the variable η in Eq. (2.9). In the mesh-refinement study, for a fixed domain, we vary the size of h, hence conventionally we choose Δx to be the same size as h so that for simplicity the number of grid points is the same as the number of particles.

On a fixed domain $[-30, 30]$, at time $t = 1$, the errors are listed in Table 5.1. As the table shows, the particle method is second-order accurate in space, consistently with the theory. For the next calculation, on a wider domain $[-50, 50]$, a single CPU on a 4-CPU DEC-Alpha (667 MHz ES40 processor) machine is used to compute the travelling wave solution up to time $t = 5$. We compare the elapsed CPU time between the fast summation algorithm and the original algorithm with different number of particles. Table 5.2 shows explicitly that the fast summation algorithm for N particles is $O(N)$, while the original straightforward algorithm is $O(N^2)$. Fig. 5.1 is a plot for the computed travelling wave solution at time $t = 20$ using both the fast summation and

Table 5.1
Convergence rate for the particle method

Δx	0.1	0.05	0.025	0.0125	0.00625
$\|u - u_{\text{exact}}\|$	6.90e − 4	1.94e − 4	4.65e − 5	1.17e − 5	3.03e − 6
Rate		1.83	2.06	1.99	1.93

Table 5.2
CPU time for the two summation algorithms

Seconds	N				
	1000	2000	4000	8000	16,000
Fast summation	1	2	4	9	19
Ratio		2	2	2.2	2.1
Original	17	74	290	1157	4505
Ratio		4.35	3.92	3.99	3.89

This table shows that the fast summation algorithm is O(N), and the straightforward algorithm is O(N^2), where N is the number of particles.

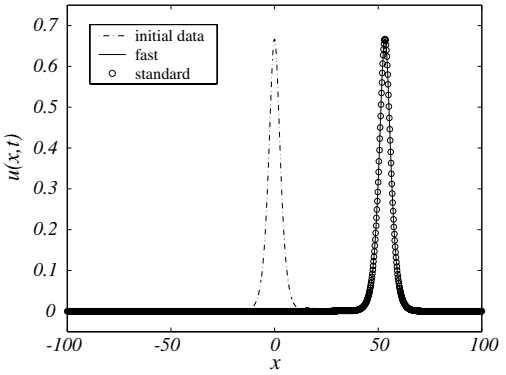

Fig. 5.1. Numerical simulations of the travelling wave solution (5.1) with $\kappa = 1$ by the fast and standard summation algorithms, with $N = 1000$, $h = 0.2$, at time $t = 20$.

the standard algorithm. The numerical solutions are graphically indistinguishable, confirming that there is no discrepancy between the two algorithms except efficiency.

5.2. Sharp peaked travelling waves for $\kappa = 0$ and numerical particle collisions

In Ref. [4], a calculation using the present characteristics formulation with initial condition $m_0(x) = a\,\mathrm{sech}^2(x)$ (equivalent to $q(\xi,0) = \xi$ and $p(\xi,0) = a\,\mathrm{sech}^2(\xi)$ for the particle method) shows that a rather sharply peaked wave forms and moves to the right, followed by others emerging from the location of the initial hump m_0, a familiar behavior for this equation first observed in [7]. During the simulation, one can observe that the particles rapidly cluster in the region of the peak of the first and second solitary waves. Such pile-up phenomenon suggests that particles get very close to each other in this region. When the distance between particles is so close that the machine precision can no longer distinguish between locations of the coalescing particles, *particle collisions* occur numerically. This effect is of course purely numerical, as we have shown in Section 2.1 that particle collisions cannot take place in finite time. As a consequence of such a numerical artifact, the particle method breaks down shortly after the numerical collision occurs.

To illustrate the dominant mechanism of the numerical collision, we perform the same calculation as in [4] with three different floating point precisions. The first row in Table 5.3 shows the times when collisions occur,

Table 5.3
First collision times vs. arithmetic precision of numerics

	Single precision	Double precision	Quadruple precision
Time	54.9	140.3	317.1
$u(x = 50.6,\ t = 150)$	0.317747861146927	0.317904674362106	0.317904674362127

The second row shows the numerical value of u at the first soliton peak location $x = 50.6$ and $t = 150$. The redistribution algorithm is employed with the single and double precision arithmetics runs.

in the course of computing ps and qs, with respect to increasing precision. The table shows that higher precision arithmetic extends the time for first occurrence of particle collisions, thereby providing evidence that this phenomenon is dominated by the round-off error.

5.3. Redistribution algorithm

The concentration of particles that leads numerically to artificial collisions allows us to implement a redistribution algorithm rather efficiently: when two particles, with positions q_i and q_{i+1}, are too close to be distinguished within machine precision, we replace them with one particle at the same location carrying a momentum equal to the sum of p_i and p_{i+1}.

After carrying out this replacement, we relabel the rest of the particles from the original $i+2,\ldots,N/2$ to $i+1,\ldots,N/2-1$. Thus, we reduce the dimension of the system of ODEs from $2N$ to $2N-2$ by combining any two clustering particles. Of course, this method is somewhat crude in that the moving (Lagrangian) grid can become too sparse in regions away from the clustering particle, as this process of replacement depletes the total number of particles. While it is not too difficult to implement a true redistribution algorithm that conserves particles, we leave this out for simplicity; we find that even this crude criterion does not affect the simple tests we performed in this work, by comparing with the other PDE integral methods reported below.

As we indicate in the first row of Table 5.3, the numerical collision occurs at time $t = 54.9$ for the single precision calculation, and at $t = 140.3$ for the double precision calculation. There are no numerical collisions for the quadruple precision calculation until $t = 317.1$. We perform a calculation up to $t = 150$ at each of the three different precisions. The result from the quadruple precision calculation is used as a relative exact solution, since there are no numerical collisions for this calculation at $t = 150$. After applying the redistribution algorithm for the single and the double precision calculation, the second row of Table 5.3 lists the computed solution for u at $x = 50.6$, where the first peaked soliton is located. These values in the table show that the numerical solution obtained by using the double precision arithmetic matches the relative exact solution up to thirteen digits. The solution obtained by using the single precision arithmetic, however, has only three matching digits. It seems reasonable to attribute this discrepancy to the nonlinearity of the equation, which can amplify the round-off error and the error caused by the redistribution algorithm, since they are both influenced by the different floating-point precision used. Thus, while the same algorithm is used in the two computations, the overall errors for the numerical solutions grow nonlinearly while approaching the near-singular clustering episodes.

Fig. 5.2 is the plot of reconstructed solutions at $t = 150$ for the three different precisions. The solid line is the result from the quadruple precision. The comparison shows that solutions computed from the redistribution algorithm are graphically indistinguishable from the reference high arithmetic precision solution.

Remark 5.1. A fixed ratio $\Delta t = h/2$ is used in these simulations, where Δt is the temporal discretization and h is the spatial discretization for the Riemann sum in the ODE system (2.10). An adaptive-step-size time integrator may improve the overall efficiency and accuracy of the current algorithm, and this is currently under investigation. However, we stress that a variable step size will not prevent numerical collisions from taking place, since the step size of a time integrator is definitely independent of the "singularity" formation defined by two particles occupying the same position. The numerical experiments we have performed show that numerical collisions are in fact an artifact caused by the lack of infinite arithmetic precision, not by the stiffness of the ODE system (2.10), as summarized by Table 5.3.

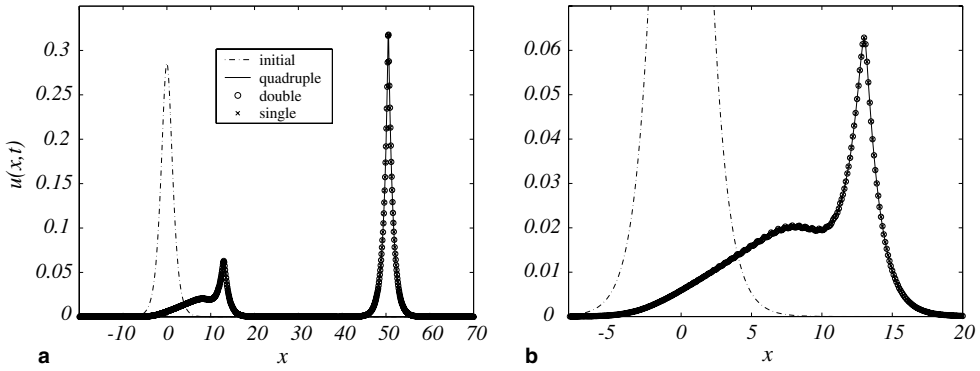

Fig. 5.2. (a) Evolution under Eq. (1.1) for $\kappa = 0$ of the initial condition (dash) $m_0(x) = a\,\mathrm{sech}^2(x)$, with $a = 1/2$ for three different precisions, at time $t = 150$. (b) Magnification of the region around the second emerging peaked solitary wave.

Remark 5.2. When the redistribution algorithm is applied to the particle method, we choose to maintain the same h for the ODE system, while the domain for the variable η is changing, due to the reduction of the particle numbers. The physical domain, however, remains unchanged, since the grid size for this domain (or the number of the grid points) is independent of the number of particles.

Remark 5.3. When the distance between particles decreases exponentially fast, this can be problematic for our particle method (or any particle method). In fact, such singular or "near-singular" formation is challenging for any numerical scheme. We believe that the right way for resolving this problem is to implement a "local collision (or quasi-collision)" model which can be then incorporated into the numerical scheme. Since our emphasis in this paper is on simplest implementation of the scheme, we leave issues of improving its efficiency to later work.

5.4. Error analysis and the constraint (2.3)

As remarked in Section 2, the field $p(\xi,t)$ is tied to $q(\xi,t)$ by the constraint (2.3). For the discretization of system (2.9) offered by the particle method, this exact relation between the p and q variable cannot survive. However, convergence of the particle method to the PDEs solution and its smoothness, inherited from appropriate classes of initial data, assure that given a certain time T there exists a step-size h such that (abusing notation a little)

$$p(\xi_i,t) = p_i(t) + \mathrm{O}(h^2) \quad \text{and} \quad p(\xi_i,t) = \frac{2hp_i^0}{q_{i+1}(t) - q_{i-1}(t) + \mathrm{O}(h^3)} \tag{5.4}$$

for all times $0 < t < T$.

Because the sharpness of the convergence estimates (3.15) is not known precisely, the practical question of how long the solution of the particle method can be trusted to stay close to that of the PDE for a given h is not addressed by the convergence proof. When an exact solution is available, it is customary to simply test the code, as we have done for the travelling wave solution, and assume that the closeness study holds for more general initial conditions where an exact solution is not known. The constraint (2.3) in its version (5.4) offers a different and more systematic way to monitor the error. In fact, apart from spurious cancellations, relations (5.4) show that the deviation

$$e_h(t) \equiv \sup_i \left| p_i(t) - \frac{2hp_i^0}{q_{i+1}(t) - q_{i-1}(t)} \right| \tag{5.5}$$

keeps track of the error between the exact PDE solution and its approximation by the particle method. We test this error monitor in the two cases of the travelling wave solution (5.1) for $\kappa \neq 0$ and the general evolution out of an initial hump for $\kappa = 0$.

For $\kappa \neq 0$, since a travelling solution is known explicitly, one can show that the corresponding solution $q(\xi,t)$ can be obtained [4] by the solution of the functional equation

$$q(\xi,t) = \xi + F(\xi) - F(q(\xi,t) - ct), \tag{5.6}$$

where the function $F(\xi)$ is determined explicitly by $U(\xi)$ in (5.1) through the anti-derivative

$$F(\xi) = \int^{\xi} \frac{U(\eta)}{c - U(\eta)}\,\mathrm{d}\eta = \log\left(\frac{(2\cos 2z - 1)\left(\sqrt{3} + 2\sin 2z\right)}{(6\cos 2z + 3)\left(\sqrt{3} - 2\sin 2z\right)}\right) \tag{5.7}$$

with $z = \arctan(e^{\xi/2})/3$, $c = 8\kappa/3$, and we have set $\kappa = 1$. Once $q(\xi,t)$ is known, $p(\xi,t)$ can be computed by (cf. Eq. (2.3))

$$p(\xi,t) = \sqrt{p(\xi,0)(m(q(\xi,t),t) + \kappa)},$$

where $m(x,t)$ is given for travelling waves by Eq. (5.2). Eq. (5.6) for $q(\xi,t)$ can be solved efficiently via a Newton iteration, allowing us to compare how the e_h-monitor (5.5) evolves with respect to the actual error-measure $\sup_i|p(\xi_i,t) - p_i(t)|$. This is shown in Fig. 5.3, where one can see that both error estimates share the same linear growth in time. Thus the error monitor $e_h(t)$ afforded by the constraint (2.3) constitutes a faithful representation of the actual error between the exact solution and the numerical solution from the particle method.

Next, we look at the error monitor $e_h(t)$ for an initial value problem with $\kappa = 0$ where an exact solution is not available. Fig. 5.4 shows that after an initial transient the error $e_h(t)$ grows nonlinearly to saturate at some (mean) constant level. This behavior is related to the evolution of the difference between ps in the definition (5.4) for each individual particle, when the first peaked wave of Fig. 5.2 forms and moves towards the right. This can be seen in the dashed curves of the figure, where this difference is plotted vs. time. Notice that for locations sufficiently far from the origin where the initial hump is located, viz. $i = 60$ and $i = 100$ in the figure, the $p_i(t)$s computed by both expressions in (5.4) relax back to zero after the passage of the first wave, and hence so does the error. Also, notice that for these particles the individual error suffers a sharp order-of-magnitude increase after an initial slow growth at about the times when the first wave reaches these particles' locations. This behavior is related to the clustering effect which we examine in more detail next.

5.5. The (avoided) singularity formation and vortex patch analogy

As remarked above, from the perspective of the particle method, the formation of the sharp (corner-like) peaks shown in Fig. 5.2 is associated with the particle clustering discussed in Section 5.2. We revisit the process of formation of corners in Fig. 5.5, by plotting the trajectories of particles in the (x,t) plane for a rather coarse grid. The clustering process acts as a high particle-density front sweeping through the computational domain.

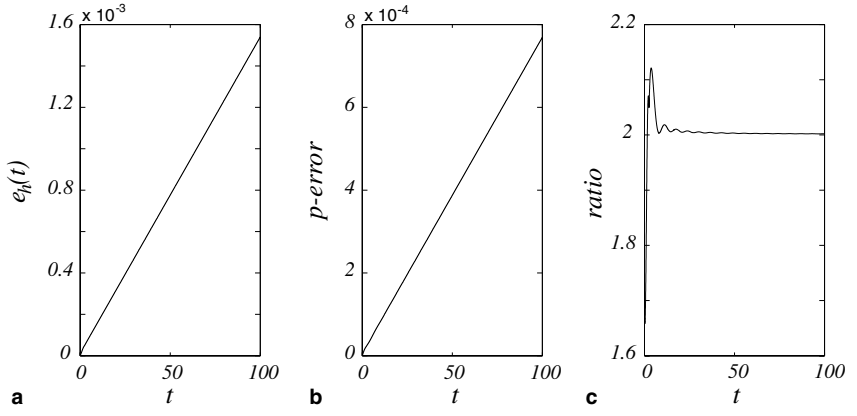

Fig. 5.3. (a) Time evolution of $e_h(t)$ for a numerical solution of Eq. (1.1) with the travelling wave initial condition (5.1). (b) Actual error $\sup_i|p(\xi_i,t) - p_i(t)|$ measured from the exact solution (5.1). (c) Ratio of the two errors: the two monitors track each other accurately after an initial transient. In this computation $N = 40{,}000$, $h = 0.025$, $\Delta t = 0.01$, and $\kappa = 1$.

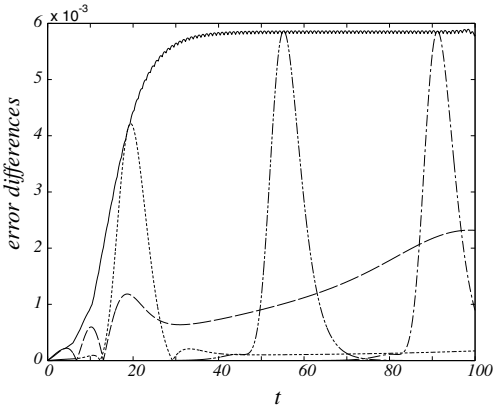

Fig. 5.4. Evolution of error differences for the initial value problem of Eq. (1.1) with $u(x,0) = 1/2\,\mathrm{sech}^2(x)$, $N = 8000$, $h = 0.1$, $\Delta t = 0.05$, and $\kappa = 0$. Solid curve: error monitor $e_h(t)$. Dashed curves: individual particle error $|p_i(t) - 2hp_i^0/(q_{i+1}(t) - q_{i-1}(t))|$, with $i = 10$ (long-dashed), $i = 20$ (short-dashed), $i = 60$ (long-short-short-dashed), $i = 100$ (long-short-dashed).

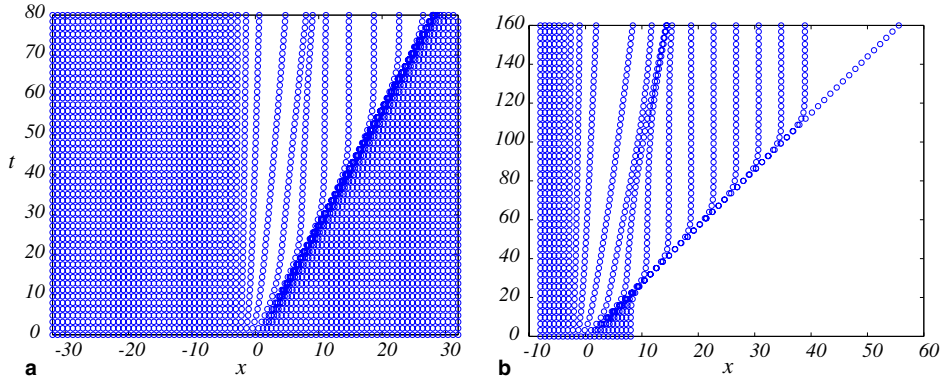

Fig. 5.5. (a) Particle trajectories on the (x,t) plane for the particle method. Here $h = 0.8$, $N = 81$ and the final time is $t = 80$. The shock-like wave of high particle-density sweeping through the domain at speed $\sim 1/3$ can be clearly seen, as well as the next incipient collision near $x = 10$. (b) Same as (a) with fewer particles $N = 21$; the momentum of the front seen at $t \simeq 15$ is completely transferred to the last (21st) particle around $t = 110$. Also seen in this plot is the formation of the second front corresponding to the new emerging peaked wave at $t \simeq 130$.

This front corresponds to the first peaked solitary wave of Fig. 5.2. The trailing edge of this quasi-shock wave leaves behind a rarefaction wave. Particles in the rarefaction wave region interact again and form the next clustering of particles, corresponding to the next peaked wave of Fig. 5.2; the onset of this second clustering can be seen at the final time in Fig. 5.5(a). (Notice that this rarefied area can increase errors due to lack of resolution, especially when coupled with a redistribution algorithm that depletes the total number of particles.)

In the computation of Fig. 5.5(a), the front in its steady motion sweeps particles from the leading edge at the rate of one every two time units, while leaving behind one particle per ten time units. Clearly, at this rate the particle density of the moving front is destined to increase, eventually leading to numerical blow-up if a redistribution algorithm is not used. However, for a finite number of particles and a given floating-point precision, it may happen that the front approaches the last particle (the edge of the initial domain) before numerical blow-up occurs. This is illustrated by Fig. 5.5(b), where we have reduced the number of particles N keeping h fixed and doubled the time of integration. In this case the momentum from the high density front is finally transferred to the right-most particle, which eventually breaks free travelling at the constant speed of the front. Thus, redistribution by replacement of several clustering particles with a single one carrying the cluster's total momentum is automatically part of the long time asymptotic for any finite N, and in fact it can be described through the complete integrability of system (2.10). Asymptotic results [4] show that for $\kappa = 0$ *all*

particles eventually spread out travelling at different (asymptotic) decreasing speeds. However, front formation occurs at intermediate time scales and as such requires a different, and possibly challenging, approach for its analysis.

The mapping $x = q(\xi,t)$ offers another interpretation of the formation of corners: the collision of two nearest-neighbor particles is the discrete counterpart of the vanishing of the Jacobian $|q_\xi(\xi,t)|$. Loss of smoothness in the form of a corner singularity at time $t = T_s$ for the solution $u(x,t)$, as suggested by the numerical solution depicted in Fig. 5.2, would imply that $|\partial_x^2 u(x,t)| \to \infty$ at some location x for $t \uparrow T_s$. In fact, from the definition (2.8) of the momentum-like variable $p(\xi,t)$, we have

$$u_{xx}(x,t) = u(x,t) - m(x,t) = u(q(\xi,t),t) + \kappa - \frac{m_0(\xi)}{(q_\xi(\xi,t))^2}, \tag{5.8}$$

showing explicitly that $q_\xi(\bar{\xi},t) \to 0$ at some $\xi = \bar{\xi}$ drives the second derivative of the velocity u to infinity at the location $\bar{x} \equiv q(\bar{\xi},t)$, for bounded u. Thus, having control on the decay of the Jacobian $|q_\xi(\xi,t)|$ of the mapping $x = q(\xi,t)$ allows control on the loss of smoothness of u in the form of infinite curvature, as is the case with corner-peaked waves. (Similarly, one can show that controlling the growth of the Jacobian $|q_\xi(\xi,t)|$ allows to rule out the formation of shock-like singularities of u.) Of course, vanishing of the Jacobian $|q_\xi(\xi,t)|$ implies crossing of characteristics for Eq. (1.1), in itself a phenomenon usually associated with formation of shocks in hyperbolic PDEs. Thus, the emergence of sharply peaked waves can also be viewed as tendency of the solution to form a shock for the non-dispersive case $\kappa = 0$, which however is prevented from fully forming in finite times.

As we have shown in Section 2.1, the bounds (2.18) on the momenta ps prevent particles from colliding. There is a PDE counterpart of these bounds showing that true characteristic crossings for Eq. (1.1) can only be achieved in infinite time. From the antisymmetry of the kernel in Eq. (2.9b), the bounds

$$m_0(\xi)\mathrm{e}^{-t\int_{-\infty}^{\infty} m_0(\xi)\,\mathrm{d}\xi} \leqslant p(\xi,t) \leqslant m_0(\xi)\mathrm{e}^{t\int_{-\infty}^{\infty} m_0(\xi)\,\mathrm{d}\xi}, \tag{5.9}$$

can be derived [4] for $\kappa = 0$ and positive initial condition $m_0(\xi)$. From the constraint (2.8), it follows that the approach of $|q_\xi(\xi,t)|$ to zero and infinity can at most be exponentially fast. Of course, for the numerics exponential smallness (as time increases) of the inter-particle distance becomes rapidly indistinguishable from true collisions.

As touched upon in Section 1, our particle method for Eq. (1.1) offers a one-dimensional cartoon of the point vortex method for incompressible Euler equations. Perhaps the best illustration of this analogy is offered by the contour dynamics of two-dimensional vortex patches (regions of uniform distribution of vorticity), whose boundary $z(\alpha,t)$ evolves according to the so-called contour dynamics equation (CDE) [32]:

$$\begin{aligned} \dot{z}(\alpha,t) &= \frac{1}{2\pi}\int_0^{2\pi} \log|z(\alpha,t) - z(\beta,t)|\omega(\beta,t)\,\mathrm{d}\beta, \\ \dot{\omega}(\alpha,t) &= \frac{1}{2\pi}\int_0^{2\pi} \Re\left(\frac{\omega(\alpha,t)}{z(\alpha,t) - z(\beta,t)}\right)\omega(\beta,t)\,\mathrm{d}\beta. \end{aligned} \tag{5.10}$$

Here the complex variable $z(\alpha,\cdot)$ maps the unit circle into a closed curve in $\mathbb{R}^2$, and the auxiliary variable $\omega(\alpha,t)$ is simply the derivative of the mapping

$$\omega(\alpha,t) \equiv \partial_\alpha z(\alpha,t).$$

Thus, the second equation is obtained by differentiating the first with respect to the curve parameter, and the time evolution constrains ω to z, just as for the q,p system (2.2).

Apart from special cases (see, e.g. [25]), numerical simulations of the CDE show that the contour evolves into highly convoluted patterns which quickly increase the contour's length and maximum curvature. This is suggestive of singularity formation in finite time out of smooth initial data, a conjecture that sparked a debate in the literature (see, e.g. [3,19,24,15]) before the matter was settled in Refs. [8,2]. The proof of global regularity of the solutions of the CDE [25] relies crucially on the control of the magnitude of the tangent vector $z_\alpha(\alpha,t)$, which plays the same role as $q_\xi(\xi,t)$ for the q,p system. In fact, $|z_\alpha(\alpha,t)|$ turns out to be bounded as in estimates (5.9), but with the simple exponentials of time now replaced by super-exponentials [25], making this case even harder to distinguish numerically from truly singular behavior.

6. Integral formulations

The particle method relies on the special mathematical features of the evolution equation (1.1). Alternative numerical algorithms for solving the initial value problem for this equation exist, of course, the most popular being perhaps those based on the pseudospectral scheme, in which spatial derivatives are approximated by Fourier transform in a periodic domain. While relatively simple to implement, Fourier based schemes suffer from the drawback of having to work with domains large enough to make the effects of periodic boundary conditions negligible.

In this section we discuss a different approach, by studying two integro-differential formulations that are equivalent to the shallow-water wave equation (1.1). These formulations show better numerical stability properties that allow us to implement simple and efficient algorithms for solving Eq. (1.1), and, furthermore, they can be used to analyze its initial *boundary* value problem.

6.1. The integro-differential equations

Consider the shallow-water wave equation (1.1) with vanishing boundary conditions at infinity. The equivalent formulation introduced in Section 2 highlights the role of the auxiliary dependent variable

$$m(x,t) \equiv (1-\partial_x^2)u(x,t) \tag{6.1}$$

with the expression

$$m_t = -2(m+\kappa)u_x - um_x$$

of Eq. (1.1). The variable u is recovered by the convolution

$$u(x,t) = \int_{-\infty}^{\infty} G(x,y)m(y,t)\,\mathrm{d}y, \tag{6.2}$$

where $G(x,y) = e^{-|x-y|}/2$ is the Green's function associated with the operator $(1-\partial_x^2)$. With (6.2), Eq. (2.7) can be written as an integro-differential equation which we call the m-formulation

$$m_t = -2(m+\kappa)\int_{-\infty}^{\infty} G_x(x,y)m(y,t)\,\mathrm{d}y - m_x\int_{-\infty}^{\infty} G(x,y)m(y,t)\,\mathrm{d}y. \tag{6.3}$$

Alternatively, moving all the terms independent of the t-derivative in (1.1) to the right hand side of the equation, we obtain

$$(1-\partial_x^2)u_t = -2\kappa u_y - 3uu_y + 2u_yu_{yy} + uu_{yyy}. \tag{6.4}$$

By the convolution formula (6.2), we express u_t as

$$u_t = \int_{-\infty}^{\infty} G(x,y)(-2\kappa u_y - 3uu_y + 2u_yu_{yy} + uu_{yyy})\,\mathrm{d}y. \tag{6.5}$$

Using integration by parts along with zero boundary conditions at infinity, we obtain an integro-differential equation,

$$u_t = -uu_x + \int_{-\infty}^{\infty} \partial_y G(x,y)\left(u^2 + \frac{u_y^2}{2} + 2\kappa u\right)\mathrm{d}y, \tag{6.6}$$

which we will refer to as the *u-formulation*. Notice that this form of the equation again displays a similarity with the Euler systems for an incompressible fluid [14], which becomes even more evident when the symmetry of the Green's function $G(x,y)$ is used, $\partial_y G = -\partial_x G$, so that the equation becomes

$$u_t + uu_x = -\partial_x\int_{-\infty}^{\infty} G(x,y)\left(u^2 + \frac{u_y^2}{2} + 2\kappa u\right)\mathrm{d}y. \tag{6.7}$$

The right hand side is the gradient of a nonlocal operator acting on a quadratic form of u, much the same as the pressure term enters the Euler equations, once pressure is eliminated via incompressibility via the Laplacian inverse acting on a quadratic form of the velocity.

It is worth pointing out that for the initial value problem the m-formulation is equivalent to the u-formulation. Given initial data $u_0(x)$, one can solve the u-formulation, or find $m_0(x)$ and then solve the m-formulation. Vice versa, if the initial data $m_0(x)$ are given, through (6.2) one can find the initial data for the u-formulation. Nonetheless, for the initial boundary value problems the m-formulation may not be optimal, even for the special case illustrated in the following section, because it is unclear in general how to assign the boundary conditions for the auxiliary dependent variable m when only boundary data for u are assigned.

6.2. Higher-order schemes

Both integral formulations have only first derivatives of time, and hence Eqs. (6.3) and (6.6) can be easily solved by the method of lines. When a simple explicit scheme is used to solve the integral formulations, the stability constraint is relaxed, due to the lack of higher-order spatial derivatives. A relatively large time step can be chosen for the time discretization in a simple explicit scheme. For instance, a typical ratio $\Delta t/h = 1/2$ is used throughout our numerical examples, compared with $\Delta t/h = 1/15$ used for the KdV equation in [11]. Thanks to the fast summation algorithm developed in Section 4, the computational cost for evaluating the integrals is $O(N)$, where N is the number of grid points. Hence the cost for solving the integro-differential formulations by the method of lines is lower than the cost of $O(N\log N)$ for solving Eq. (1.1) by the Fourier method.

To design numerical schemes based on the two formulations, we apply a simple explicit Runge–Kutta method as the time integrator. In the spatial direction, both u_x and m_x are approximated by finite difference schemes, up to the desired order. For the convolutions, the trapezoidal rule can be used for a second-order scheme. Notice that when the integrand is compactly supported, with a little extra effort one can have a higher-order numerical quadrature for the integrals, including the integrals in the particle method. The idea is to apply a local correction to the standard trapezoidal rule by using the following formulae:

Proposition 6.1. *Assume the function $f(x) \in C^\infty(\mathbb{R})$ is compactly supported in $[-Nh/2, Nh/2]$, then for $x = jh$, $j = -N/2, \ldots, N/2$, the following approximations hold,*

$$\int_{-\infty}^{\infty} e^{-|x-y|} f(y)\,dy = h\left(\sum_{k=-N/2}^{N/2} e^{-|x-kh|} f(kh)\right) - \frac{h^2}{6} f(x) + O(h^4) \tag{6.8}$$

and

$$\int_{-\infty}^{\infty} \operatorname{sgn}(x-y) e^{-|x-y|} f(y)\,dy = h\left(\sum_{k=-N/2}^{N/2} \operatorname{sgn}(x-kh) e^{-|x-kh|} f(kh)\right) - \frac{h^2}{6} f'(x) + O(h^4), \tag{6.9}$$

where h is the spatial step size and sgn *is the sign function. Note that the standard trapezoidal rule without correction terms is second order.*

Similar local correction strategies have been used in the literature [1,22,28,30] to derive higher order numerical quadratures for weakly singular and singular integrals.

We will refer to the algorithms using the integro-differential formulations as the integral equation methods (IEM). These methods are very competitive with existing finite difference and finite element methods when accelerated by fast convolution algorithms.

6.3. Numerical examples

To validate the numerical implementation and test for the order of convergence of the integral equation methods, we look again at the traveling wave example in Section 5. The numerical solution obtained is

compared with the exact solution of Eq. (1.1). We show the results of a second-order scheme using the u-formulation, and that of a fourth-order scheme using the m-formulation. For both schemes, the time integrator is a uniform-step fourth-order Runge–Kutta method. Table 6.1 shows the result of the second-order scheme and Table 6.2 is the result from the fourth-order scheme. For both tables, the error is estimated by the 2-norm defined in (5.1). With the same order, our numerical experiments show the results obtained from the two formulations have little or no difference.

When $\kappa = 0$, for positive initial data there are no particle collisions in finite time. Nevertheless, we have seen in the previous sections that for these initial data sharply peaked (corner-like) waves quickly develop. Such phenomenon poses a challenge for the integral equation methods, since a fine grid is necessary to resolve the solution near the peak. An ideal integral equation method should include some adaptive mesh refinement algorithm to overcome this problem while maintaining efficiency. The particle method, in contrast, can use a relatively coarse particle-distribution initially with the numerical solution capturing corner-peaked waves at later times, with particles naturally clustering near the peak. However, this has the disadvantage of generating numerical collisions, which adds the extra cost of a redistribution algorithm.

Fig. 6.1 illustrates these differences between the particle and integral methods by focusing on the numerical solution for the second emerging peaked wave in the $\kappa = 0$ case. Fig. 6.1(a) shows the solutions computed by the integral method with four increasingly refined grids. As one can see, significant differences are generated by grid refinement. In contrast, Fig. 6.1(b) shows that for the particle method the solution obtained from coarse-distributed initial data is consistent with the one obtained from the fine-distributed initial data, and is identical with the solution computed by the integral equation method using the finest grid in Fig. 6.1(a). This experiment shows that the particle method may be preferable for this case of emerging sharp-peaked waves.

Table 6.1
Convergence rate for the second-order scheme using the u-formulation

h	0.1	0.05	0.025	0.0125	0.00625
$\|u - u_{\text{exact}}\|$	9.20e − 4	2.30e − 4	5.75e − 5	1.44e − 5	3.60e − 6
Rate		2.00	2.00	2.00	2.00

Table 6.2
Convergence rate for the fourth-order scheme using the m-formulation

h	0.1	0.05	0.025	0.0125	0.00625
$\|u - u_{\text{exact}}\|$	9.52e − 7	5.96e − 8	3.73e − 9	2.33e − 10	1.46e − 11
Rate		4.00	4.00	4.00	4.00

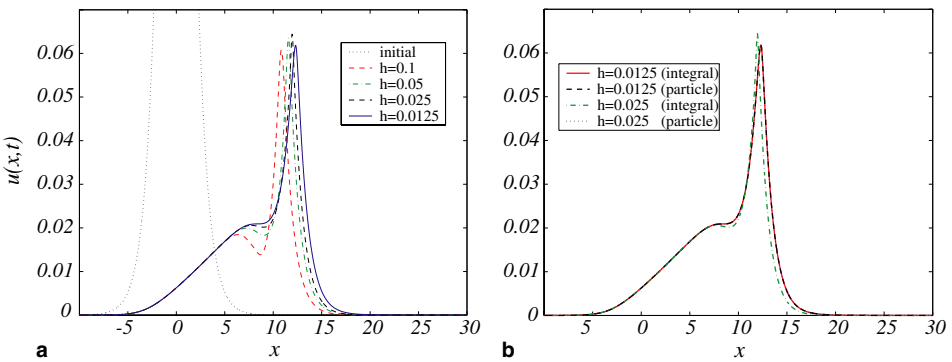

Fig. 6.1. (a) The second emerging soliton for the case $\kappa = 0$. Numerical solutions obtained from the integral equation method, using uniform grids. Coarser grids are noticeable different from the finest grid. (b) The coarse-grid numerical solution using the particle method is indistinguishable with the fine-grid solutions computed by both integral and particle methods.

7. An initial-boundary value problem

The "quarter-plane problem" for Eq. (1.1) is obtained by restricting x to the positive semi-axis and assuming boundary conditions at $x = 0$ and for $x \to \infty$, besides the initial condition $u(x,0) = f(x)$. For physical applications, it is natural to impose $u(x,t) \to 0$ as $x \to \infty$ together with any number of derivatives for any finite time t. At $x = 0$ the situation is more delicate: it is not immediately obvious how many boundary conditions one must assume without overdetermining the problem.

A complete discussion of the initial-boundary value problem is beyond the scope of this paper (a more complete study is in preparation). In this section, we will only show that assigning the boundary condition $u(0,t) = g(t)$, where $g(t)$ is some smooth function of time with $g(t) \leqslant 0$ for all t, is enough to guarantee uniqueness of the solution. Clearly, this must also constitute a minimal set of boundary conditions. As usual, we work with the special case $\kappa = 0$ knowing that this restriction can be relaxed with little extra effort. Both the particle and the integral infinite-line algorithms can easily be adapted to deal with this class of boundary value problems, and we demonstrate this in Section 7.1 with an example of numerical solution.

Proposition 7.1. *Consider the shallow-water wave equation* (1.1) *posed in a quarter plane*, $x \geqslant 0$. *Assume that a strong solution* $u(x,\cdot)$ *exists in* $H^4(0,\infty)$, *where* H^n *is the Sobolev space of* (*real valued*) *functions f on the positive real line*, $\int_0^\infty \sum_{k=0}^n |f^{(k)}(x)|^2 \,\mathrm{d}x < \infty$. *Suppose smooth initial data* $u(x,0) = f(x)$ *and smooth boundary data at* $x = 0$, $u(0,t) = g(t)$, *are given and are compatible at the origin*, $g(0) = f(0)$. *If* $g(t) \leqslant 0$ *the solution is unique for all times of existence.*

Proof. Assuming $\kappa = 0$ in Eq. (2.7), we argue by contradiction. Suppose that there exist two (strong) solutions $u_1(x,t)$ and $u_2(x,t)$ for the same data together with their auxiliary fields $m_1(x,t)$ and $m_2(x,t)$, respectively. The evolution equation for the difference variables $u(x,t) = u_1(x,t) - u_2(x,t)$, $m(x,t) = m_1(x,t) - m_2(x,t)$ is

$$m_t = -2(m_1 u_{1x} - m_2 u_{2x}) - (u_1 m_{1x} - u_2 m_{2x}) = -2(m u_{1x} + m_2 u_x) - (u m_{1x} + u_2 m_x).$$

Interchanging the indexes 1 and 2 in this expression generates

$$m_t = -2(m u_{2x} + m_1 u_x) - (u m_{2x} + u_1 m_x)$$

and summing these two expressions for m_t yields

$$m_t = -2(m\bar{u}_x + \bar{m}u_x) - (u\bar{m}_x + \bar{u}m_x), \tag{7.1}$$

where we have defined the averages

$$\bar{u} \equiv \frac{u_1 + u_2}{2}, \quad \bar{m} \equiv \frac{m_1 + m_2}{2}.$$

Thus, the linearized form of Eq. (2.7) around the algebraic mean of the hypothetical multiple solutions, Eq. (7.1), governs the evolution of $u(x,t)$ with homogeneous initial and boundary data $u(x,0) = 0$ and $u(0,t) = 0$. Estimates on the evolution of the H^1-norm $\|u\|_1$ can be obtained by multiplying (7.1) by $u(x,t)$ and integrating both sides of the equation. After integration by parts and taking into account the homogeneous boundary condition $u(0,t) = 0$, we get

$$\frac{1}{2}\partial_t \|u\|_1^2 = -\int_0^\infty \left(\frac{3}{2}\bar{u}_y u^2 + \frac{1}{2}\bar{u}_y u_y^2 - \frac{1}{2}\bar{u}_{yyy} u^2\right) \mathrm{d}y + \frac{1}{2}\bar{u}(0,t) u_x^2(0,t). \tag{7.2}$$

The integral term can be easily bounded by the H^1-norm and the sup-norm on $\bar{u}_x$ and $\bar{u}_{xxx}$ (or $\bar{m}_x$, which are all controlled by the H^4-norm, assumed to be finite for the two solutions u_1 and u_2), so that

$$\|u(\cdot,t)\|_1^2 \leqslant C \int_0^t \|u(\cdot,s)\|_1^2 \,\mathrm{d}s + \int_0^t g(s) u_x^2(0,s) \,\mathrm{d}s, \tag{7.3}$$

where the constant C is

$$C = \sup_{s\in[0,t]} \{3|\bar{u}_x|_\infty(s), |\bar{u}_{xxx}|_\infty(s)\}$$

and we used the boundary condition $\bar{u}(0,t) = g(t)$. The case $g(t)$ non-positive is manifestly handled with inequality (7.3), since the last (inhomogeneous) term generated by the boundary condition can be dropped if $g(t) \leqslant 0$ while maintaining the inequality. Applying Gronwall's lemma, and taking into account the initial condition $u(x,0) = 0$, shows that $\|u(\cdot,t)\|_1 = 0$, which contradicts the assumption of existence of two distinct (strong) solutions u_1 and u_2. □

7.1. Numerical experiments

Just as for the real line initial-value problem, it is convenient to rewrite Eq. (1.1) on the half-line in a form more convenient for implementing a numerical scheme. The counterpart of the integro-differential equation (6.5) for the half-line is

$$u_t = \int_0^\infty G_0(x,y)(-2\kappa u_y - 3uu_y + 2u_y u_{yy} + uu_{yyy})\,\mathrm{d}y + g\prime(t)\mathrm{e}^{-x}, \tag{7.4}$$

where $G_0(x,y)$ is the domain Green's function with homogeneous Dirichlet boundary condition,

$$G_0(x,y) = \frac{1}{2}(\mathrm{e}^{-|x-y|} - \mathrm{e}^{-x-y}). \tag{7.5}$$

After integration by parts, (7.4) becomes

$$u_t = \int_0^\infty \partial_y G_0(x,y)\left(u^2 + \frac{1}{2}u_y^2 + 2\kappa u\right)\mathrm{d}y - uu_x + g(t)u_x(0,t)\mathrm{e}^{-x} + g\prime(t)\mathrm{e}^{-x}. \tag{7.6}$$

One can show that the kernel of the integral in (7.6) is zero at $x = 0$, so that this form of the equation is consistent at the boundary. However, notice that knowledge of the derivative $u_x(0,t)$ at the boundary is required, though based on Proposition 7.1 this should overdetermine the problem when $g(t) \leqslant 0$. For the special case $g(t) \equiv 0$, we recover a form of the equation which is similar to (6.6); in particular $u_x(0,t)$ is not required (for smooth solutions), in agreement with the uniqueness result.

For the particle method, a formulation equivalent to (7.6) is:

$$\begin{aligned} q_t(\xi,t) &= -\kappa + \frac{1}{2}\int_\Xi^\infty \left(\mathrm{e}^{(-|q(\xi,t)-q(\eta,t)|)} - \mathrm{e}^{(-q(\xi,t)-q(\eta,t))}\right)p(\eta,t)\,\mathrm{d}\eta, \\ p_t(\xi,t) &= \frac{1}{2}p(\xi,t)\int_\Xi^\infty \left(\mathrm{sgn}(\xi-\eta)\mathrm{e}^{(-|q(\xi,t)-q(\eta,t)|)} - \mathrm{e}^{(-q(\xi,t)-q(\eta,t))}\right)p(\eta,t)\,\mathrm{d}\eta, \end{aligned} \tag{7.7}$$

where the location $\Xi(t)$ is defined by $q(\Xi(t),t) = 0$. For the special case $g(t) \equiv 0$, we have $\frac{\mathrm{d}\Xi}{\mathrm{d}t} = 0$ and hence $\Xi = 0$ at all time.

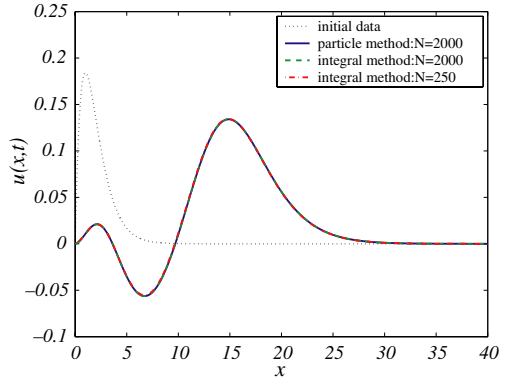

Fig. 7.1. Snapshots of numerical solutions of particle and integral equation methods for the initial-boundary value problem (7.7), with $g(t) = 0$, $\kappa = 1$, $u(x,0) = x\mathrm{e}^{-x}/2$, and different grid sizes $h = 40/N$, $N = 250$ and $N = 2000$, at time $t = 8$. The three different snapshots are graphically indistinguishable, suggesting that the numerics converge to the unique solution.

Table 7.1
The difference between numerical solutions of the second-order particle method and integral equation method in the infinity and l_2 norms, respectively, for the initial-boundary value problem (7.7), with $g(t) = 0$, $\kappa = 1$, and $u(x,0) = x\mathrm{e}^{-x}/2$

h	0.025	0.0125	0.00625	0.003125	0.0015625
$\|u_{\text{particle}} - u_{\text{integral}}\|_\infty$	1.80e − 5	4.52e − 6	1.13e − 6	2.89e − 7	7.38e − 8
Ratio		3.99	4.00	3.92	3.91
$\|u_{\text{particle}} - u_{\text{integral}}\|_2$	3.61e − 6	9.20e − 7	2.31e − 7	5.61e − 8	1.42e − 8
Ratio		3.92	3.97	4.12	3.94

The computational domain is $[0, 50]$ with a uniform grid of size h, and the final time is $t = 2$. Decreasing the grid size from h to $h/2$ decreases the difference between the two solutions by a factor of 1/4.

We use the integral and particle formulations, (7.6) and (7.7), respectively, in a numerical simulation that illustrates our analysis for the initial boundary value problem of the nonlinear shallow-water wave equation (1.1). We take the initial condition $u(x,0) = f(x) = x\mathrm{e}^{-x}/2$ (so that $m_0(x) = \mathrm{e}^{-x}$) and homogeneous boundary condition $g(t) = 0$ at $x = 0$. Snapshots of the solution after some time by the different algorithms are shown in Fig. 7.1. The solutions computed by the two different methods converge to each other, and the convergence rate is quadratic for both methods, in accordance to their order and with the uniqueness of solutions for homogeneous boundary data on u. The convergence test is documented by Table 7.1, where the difference between the solution $u(x,t)$ computed by the integral equation method and that reconstructed from the particle method is computed at a fixed time vs. decreasing grid size h.

We remark that numerical solutions (using the integral method with $u_x(0,t)$ defined by one-sided finite differencing) for non-trivial functions $g(t)$ achieve similar results for the case $g(t) \leqslant 0$, but fail to pass the necessary convergence test for positive data. Results for the general case will be reported in a separate paper.

8. Concluding remarks

We have examined in detail two integration algorithms for an evolution equation modelling long waves at the surface of water. Both algorithms take advantage, and are based on, a special structure of the equation. The model is particularly useful as a relatively simple example where analysis and numerics can be pushed to a high degree of detail, including a proof of convergence of the particle based numerical scheme, while still supporting non-trivial behavior, such as the near-singular evolution, which serves to illustrate the need for care when interpreting numerical observations. We kept the emphasis on simplicity of the schemes, rather than efficiency, but provided several pointers throughout this work where natural extensions could greatly improve the performance of our algorithms.

Acknowledgments

R.C. gratefully acknowledges support from NSF through Grant DMS-0104329, and from DOE CCPP and BES programs during some of the early stages of this work. J.H. is supported by NSF Grant DMS-0327896; part of the work was finished while J.H. was a visiting scholar at the National Center for Theoretical Sciences at Tsing Hua University, Hsinchu, Taiwan, R.O.C., and their support is thankfully acknowledged. L.L. is grateful to the Department of Mathematics and the Applied Mathematics Group at the University of North Carolina at Chapel Hill for their support through a postdoctoral fellowship. We thank the anonymous referees for pointing out that the issue of stiffness in singularity formation needed clarification.

References

[1] B.K. Alpert, Hybrid Gauss-trapezoidal quadrature rules, SIAM J. Numer. Anal. 20 (1999) 1551–1584.
[2] A.L. Bertozzi, P. Constantin, Global regularity for vortex patches, Commun. Math. Phys. 152 (1993) 19–28.
[3] T.F. Buttke, The observation of singularities in the boundary of patches of constant vorticity, Phys. Fluids A 1 (1989) 1283–1285.
[4] R. Camassa, Characteristics and the initial value problem of a completely integrable shallow water equation, DCDS-B 3 (2003) 115–139.

[6] R. Camassa, A.I. Zenchuck, On the initial value problem for a completely integrable shallow water wave equation, Phys. Lett. A 281 (2001) 26–33.
[7] R. Camassa, D.D. Holm, J.M. Hyman, A new integrable shallow water equation, Adv. Appl. Math. 31 (1993) 23–40.
[8] J.-Y. Chemin, Persistance de structures geometriques dans les fluids incompressibles bidimensionnels, Ann. Ec. Norm. Supér. 26 (1993) 1–16.
[9] H.W. Cheng, J.F. Huang, T. Leiterman, An adaptive fast solver for the modified Helmholtz equation in two dimensions, J. Comput. Phys. 211 (2006) 616–637.
[10] A. Chertock, D. Levy, Particle methods for dispersive equations, J. Comput. Phys. 171 (2001) 708–730.
[11] C.K. Chu, L.W. Xiang, Y. Baransky, Solitary waves induced by boundary motion, Commun. Pure Appl. Math. XXXXVI (1983) 505–528.
[12] E.A. Coddington, N. Levinson, The Theory of Ordinary Differential Equations, Krieger, Malabar, FL, 1984.
[14] A. Constantin, H.P. McKean, A shallow water equation on the circle, Commun. Pure Appl. Math. 52 (1999) 949–982.
[15] P. Constantin, E.S. Titi, On the evolution of nearly circular vortex patches, Commun. Math. Phys. 119 (1988) 177–198.
[19] D.G. Dritschel, M.E. McIntyre, Does contour dynamics go singular? Phys. Fluids A 2 (1990) 748–753.
[20] L. Greengard, J.F. Huang, A new version of the Fast Multipole Method for screened Coulomb interactions in three dimensions, J. Comput. Phys. 180 (2002) 642–658.
[22] S. Kapur, V. Rokhlin, High-order corrected trapezoidal quadrature rules for singular functions, SIAM J. Numer. Anal. 34 (1997) 1331–1356.
[23] Y. Kodama, K.T.-R. McLaughlin, Explicit integration of the full symmetric Toda hierarchy and the sorting property, Lett. Math. Phys. 37 (1996) 37–47.
[24] A. Majda, Vorticity and the mathematical theory of incompressible fluid flow, Commun. Pure Appl. Math. 39 (1986) 5187–5220.
[25] A.J. Majda, A.L. Bertozzi, Vorticity and Incompressible Flow, Cambridge University Press, Cambridge, 2002.
[26] J. Moser, Finitely many mass points on the line interacting under the influence of an exponential potential – an integrable system, Lect. Notes Phys. 38 (1975) 467–497.
[27] O. Ragnisco, M. Bruschi, Peakons, *r*-matrix and Toda lattice, Physica A 228 (1996) 150–159.
[28] V. Rokhlin, End-point corrected trapezoidal quadrature rules for singular functions, Comput. Math. Appl. 20 (1990) 51–62.
[29] J.A. Sanders, F. Verhulst, Averaging Methods in Nonlinear Dynamical Systems, Springer-Verlag, Germany, 1985.
[30] J. Strain, Locally corrected multidimensional quadrature-rules for singular functions, SIAM J. Numer. Anal. 16 (1995) 992–1207.
[32] N.J. Zabusky, M.H. Hughes, K.V. Roberts, Contour dynamics for the Euler equations in two dimensions, J. Comput. Phys. 48 (1979) 96–106.
[34] V. Zeitlin, S.B. Medvedev, R. Plougonven, Frontal geostrophic adjustment, slow manifold and nonlinear wavephenomena in one-dimensional rotating shallow water. Part I. Theory, J. Fluid Mech. 481 (2003) 269–290.